Received: 25 November 2021 | Revised: 4 March 2022 | Accepted: 7 March 2022

DOI: 10.1002/er.7860

REVIEW PAPER

INTERNATIONAL JOURNAL OF ENERGY RESEARCH WILEY

The microencapsulation, thermal enhancement, and applications of medium and high-melting temperature phase change materials: A review

Rizal Sinaga[1,2] | Jo Darkwa[1] | Siddig A. Omer[1] | Mark Worall[1]

[1]Faculty of Engineering; Building, Energy and Environment Research Group, University of Nottingham, University Park, Nottingham, UK

[2]Engineering Management Study Program, Institut Teknologi Del, Laguboti, Indonesia

Correspondence
Rizal Sinaga, Faculty of Engineering, Building, Energy and Environment Research Group, University of Nottingham, University Park, NG7 2RD Nottingham, UK.
Email: rizal.sinaga@nottingham.ac.uk; rizal.sinaga@del.ac.id

Funding information
Ministry of Education and Culture Republic of Indonesia

Summary

Microencapsulated phase change materials (MEPCMs) have made tremendous advancements in recent years, owing to their increased demand for a variety of energy storage applications. In this paper, current microencapsulation techniques, enhancement, and use of medium- and high-melting phase change materials (PCMs) are reviewed, as well as their potential benefits and limitations. The most frequently employed PCMs for medium- and high-temperature applications were recognized as salt-based, metallic, inorganic compound, and eutectic. Meanwhile, polymethyl methacrylate (PMMA), polystyrene-butylacrylate (PSBA), polyethyl-2-cyanoacrylate (PECA), and polyurethane were widely used as polymer shell materials for encapsulating medium- and high-melting point PCMs via chemical method, whereas inorganic silica shell was synthesized via various techniques. Hydrolysis followed by heat-oxidation treatment has been extensively studied since 2015 to encapsulate either metal or alloy within Al_2O_3 shells. Different techniques were developed to generate void between core and shell material to accommodate volume expansion during phase transition. Numerous approaches, including the incorporation of metal particles, carbon, and ceramic, have been found as ways to enhance the thermal performance of PCMs. Multiple storage arrangements were also established to be an effective way of enhancing the overall efficiency of medium-high melting PCM storage systems. Finally, the paper highlights the potential of medium- and high-melting temperature PCMs for solar power generation, solar cooking, and industrial waste heat recovering applications.

KEYWORDS

industrial waste heat, medium high-melting temperature, microencapsulation, phase change material (PCM), solar energy, thermal enhancement

1 | INTRODUCTION

Due to the rapid growth of the worldwide population, the demand for energy also abruptly and exponentially increases.[1] The huge continuous energy consumption positively affects the rise of CO_2 emission level, which contributes significantly to climate change and global warming.[2] According to the greenhouse gas (GHG) data,

fossil fuel energy system allows about 71% of global emissions in 2018.[3] Moreover, under current policies, energy-related CO_2 emission is predicted to rise by 6% between 2015 and 2055, from 33 to 35 Gigaton, as reported by Gielen et al.[4] There is therefore a need for appropriate and sustainable energy sources to be exploited if current upward trend is to be minimized.

Due to the fact that solar energy is free, plentiful, and environmentally friendly, it is often regarded as a potential technique of energy harvesting. The earth acquires an average of approximately 342 W/m^2 annually, which is equivalent to about 885 million terawatt-hours (TWh) in a year.[5] Besides solar energy, there is vast amount of industrial waste heat (IWH) resources available, which could be recovered for useful purposes. For instance, the total estimated waste heat sources available in the European Union alone is 304.13 TWh/year, with about 33% corresponding to low-temperature waste heat (200°C), 25% as medium-temperature (200°C-500°C), and 22% as high-temperature (above 500°C).[6] The use of solar energy and waste energy sources, on the other hand, are hampered by an imbalance between the available and required energy. Therefore, by storing and releasing energy, thermal energy storage (TES) has the potential to increase the energy efficiency of solar thermal systems.

Phase change materials (PCMs) have been identified as potential materials that can be used to provide effective TES systems. PCMs can store and release energy during the phase transition period as liquid-gas, solid-gas, solid-solid, or solid-liquid covering a wide temperature range.[7] Nevertheless, both liquid-gas and solid-gas PCMs are not capable of being utilized due to their enormous density and pressure changes during phase transformation processes. Solid-solid PCMs can however absorb and release energy in pseudo solid phase from crystalline/semi-crystalline phase to another amorphous, semi-crystalline, or crystalline phase without experiencing any differential changes in density and pressure. They do not also experience any leakage during phase transition, and therefore require no encapsulation but cannot easily be combined with other materials, thus limiting their application.[8] The most commonly used PCMs are the solid-liquid phase transition types because of their large heat storage density with small differential change in volume during phase transition process. They do, however, require encapsulation to protect their thermophysical and structural integrity. In addition, PCMs are commonly encapsulated in micro-scale as a technique for improving their thermal performance by increasing their surface-to-volume ratio.[9]

Microencapsulated PCM (MEPCM) with high-melting temperature potentially offers a huge energy saving in industrial applications such as solar energy and IWH recovery. Metals and alloys have been widely developed as PCMs for high-temperature applications. However, high corrosivity and heaviness restrict the use of metallic PCM to practical application, as mentioned by Li et al[10] and Zhang et al.[11] Salt-based PCMs also have attracted much attention from researchers due to their considerable phase change enthalpy, chemical stability and are economically affordable, which make them favourable candidates as high-temperature energy storage material.[12] Nevertheless, their corrosive nature and limited heat transfer abilities hinder their use field.[13] Organic PCMs are also considered as potential candidates for high-temperature applications due to the low price, high thermal storage density, good stability, and a wide range of melting temperatures.[14] However, organic PCMs do suffer from the low thermal conductivity, which tend to affect their thermal response factor during phase transition.[15] Due to the deprivations owned by PCMs, it is challenging to overcome them for achieving good thermal performance. The introduction of high thermal conductivity additive is therefore one of the techniques to improve thermal performance of composite PCMs, as reviewed by Lin et al.[16]

The selection of shell material is also an important factor when encapsulating medium and high-melting PCMs. Thermal stress produced by volume expansion occurs during phase change process from solid to liquid, which must be taken into consideration in the encapsulation process. To solve the aforementioned issues, thick shells are required; nevertheless, this could reduce heat storage density. Due to these concerns, a full analysis of medium and high melting point PCM is necessary to give detailed information on their thermophysical characteristics, microencapsulation processes, thermal enhancement, and applications.

Numerous studies have evaluated the available low to medium melting point PCMs, as well as their microencapsulation processes and implementations. Despite the wide applications of medium and high melting PCM in solar thermal power plants,[17] solar cookers[18] heating hot water systems[19]; only a few studies have explored and reviewed the accessible medium and high melting point PCMs, as reported by Zhou and Wu.[20] For instance, Zhou and Wu[20] performed a review of inorganic and metals alloys for medium- and high-temperature PCMs, including analysis of the PCMs' corrosivity and stability. Liu et al[21] reviewed PCMs with high-melting temperature over 300°C for concentrated solar thermal power plants, as well as approaches for improving their thermal performance. Costa and Kenisarin[22] provided a review article about the thermophysical properties of metallic PCM for low-, medium-, and high-melting temperatures, including their mathematical theoretical predictions. Liu et al[23] conducted a review for high-melting temperature of inorganic salt mixtures and metal alloys in the range of

500°C until 700°C. Milián et al[24] summarized the encapsulation PCM methods for a wide range melting temperature. However, it is confined to the encapsulation of inorganic PCMs. Pereira da Cunha and Eames[25] reviewed the applications and heat enhancement mechanism of PCMs with a phase transition between 0°C and 250°C. Nonetheless, coverage of their microencapsulation requires elaboration. Liu et al[26] provided a detailed review of the numerous ways for microencapsulating PCMs with a wide temperature range in a variety of organic and inorganic shell materials. Zhu et al[27] focused on a review of micro- and nano-encapsulation of metal and alloy PCMs with low- to high-melting temperature.

Comprehensive review for microencapsulation, thermal enhancement, and applications for all types of medium and high-melting PCMs, therefore, still needs to be addressed. In this regard, the objective of this paper is to review available medium- and high-melting of all types solid-liquid PCMs ranging from 80°C to 200°C and above 200°C, respectively. Additionally, this study includes a review of the microencapsulation methods for medium- and high-melting PCMs, as well as their thermal enhancement and applications.

2 | MEDIUM- AND HIGH-MELTING TEMPERATURE PCMS

This section covers a review of organic, inorganic, and eutectic types of PCMs that could be utilized for medium- and high-melting temperature energy storage applications. The classification of medium- and high-melting PCMs is displayed in Figure 1.

2.1 | Organic PCMs

Organic PCMs consist of paraffin and non-paraffin PCMs. They are non-corrosive, economical, abundant raw material, stable physical and chemical characteristics, no subcooling, high energy density, and self-nucleation capacity.[28] However, low thermal conductivity and flammability issues do restrict the application of these types of PCMs.[29]

2.1.1 | Paraffin PCMs

Paraffin is produced as a by-product of petroleum refining system. These types of PCMs have hydrocarbon formula as C_nH_{2n+2} where n is the number of carbon atom (C). Regardless of its low thermal conductivity, paraffin is extensively utilized due to the high latent heat of fusion, congruent melting, and structurally stable over many cycles.[30] Table 1 shows the thermophysical properties of available medium and high-melting paraffin PCMs.

2.1.2 | Non-paraffin PCMs

These PCMs include various materials such as fatty acids, alcohols, and glycols. The chemical formula of fatty acid is $CH_3(CH_2)_{2n}$·COOH originated from vegetables and animal, which is more reliable and cleaner sources.[34] Meanwhile, polyethylene glycols (PEGs) are composed of linear oxyethylene (—O—CH_2—CH_2—) with ending groups of hydroxyl (—OH). The melting temperature of PEG has a proportional relationship to its molecular weight.[28] PCMs based on alcohol derivatives perform solid-solid phase change, which exhibits no leakage and no phase separation issue.[35]

In general, non-paraffin PCMs can achieve solidification with very little supercooling. They also have excellent chemical stability and high latent heat of fusion. However, low thermal conductivity and flammability issues are the main drawbacks.[8] In addition, several types of non-paraffin PCMs are toxic, which therefore require encapsulation to protect the application environment.[30] Table 2 displays the thermophysical properties of available non-paraffin PCMs.

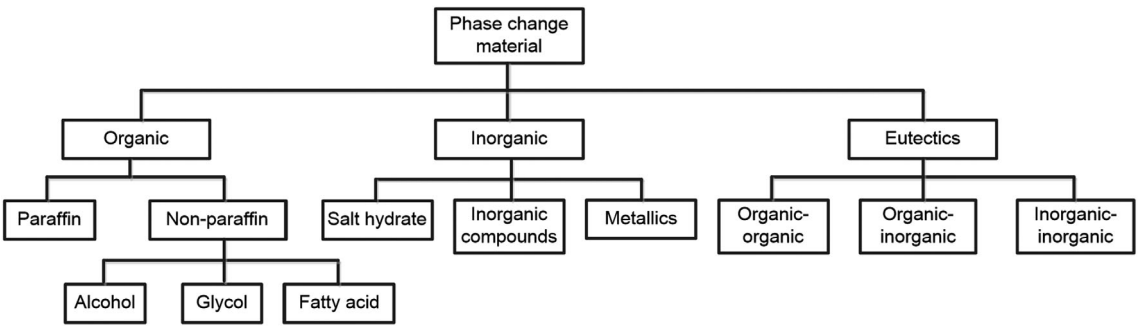

FIGURE 1 The classification of medium- and high-melting PCM

TABLE 1 Thermophysical properties of paraffin PCMs

Type of PCM	T_m (°C)	Latent heat (kJ/kg)	Specific heat capacity (kJ/kg K)	Thermal conductivity (W/m K)	Density (kg/m^3)	Reference
Paraffin natural wax 79	77 to 81	80	NA	0.63	1200	31
RT 80	85.1	161.1	NA	NA	NA	14
RT 82	82	170	2 (s)	0.2 (s,l)	880 (s), 770 (l)	32
Paraffin natural wax 84	82 to 86	85	NA	0.72	1200	31
RT 90 HC	90	170	2 (s)	0.14 (l)	950 (s), 850 (l)	32
RT 100	100	120	2 (s)	0.2 (s), 0.14 (l)	880 (s), 770 (l)	32
RT 100 HC	100	180	2 (s)	0.2 (s,l)	1000 (s), 850 (l)	32
Paraffin natural wax 106	104 to 108	80	NA	0.65	1200	31
Polyethylene	110 to 135	200	NA	NA	NA	33

TABLE 2 Thermophysical properties of non-paraffin PCMs

Type of PCM	T_m (°C)	Latent heat (kJ/kg)	Thermal conductivity (W/[m K])	Density (kg/m^3)	Reference
Methyl brombrenzoate	81	126	NA	NA	36
Acetamide	81	241	0.287 (s), 0.240 (l)	1159	37-39
Stearic acid	66 to 83	189	0.29	940	40,41
Xylitol	94	263	1.314 (s), 0.412 (l)	1500 (s)	33,42
Alpha napthol	96	163	NA	1095	37,38
D-Sorbitol	97	185	NA	1520 (s)	33
Glautaric acid	97.5	156	NA	1429	37,38
p-Xylene dichloride	100	138.7	NA	NA	37
Methyl fumarate	102	242	NA	1045	37,38
Catechol	104.3	207	0.040	1370	36,38,43
Quinone	115	171	NA	1318	37,38
Acetanilide	115	142	0.300 to 0.350	1210	38,44
Acetanilide 222	118.9	222	NA	NA	36
Succinic anhydride	119	204	NA	1104	37,38
Erythritol	120	340	0.733 (s), 0.326 (l)	1480 (s), 1300 (l)	33
Benzoic acid	121.7	142.8	0.132 to 0.139	1266	37,38,45
Stibene	124	167	NA	1164	37,38
Benzamide	127.2	169.4	NA	1341	37,38
Phenacetin	137	136.7	NA	NA	38
Alpha Glucose	141	174	NA	1544	38
Acetyl-*p*-toluidene	146	180	NA	NA	8
Phenylhydrazone benzaldehyde	155	134.8	NA	NA	8
Salicylic acid	159	199	NA	1443	38
Benzanilide	161	162	NA	NA	8
O-Mannitol	166	294	NA	1489	38
D-Mannitol	167	316	0.010 to 0.036	1520	33,46
Hydroquinone	172.4	258	NA	1358	38
p-Aminobenzoic acid	187	153	NA	NA	38
Galacticol	188	351	0.19	1520	33,47

2.2 | Inorganic PCM

The main benefits of inorganic PCMs as TES include high latent heat, relatively high thermal conductivity, non-toxicity, non-flammable, and economically attractive.[24] They however suffer from phase segregation, sub-cooling, corrosive, and lack of thermal stability.[48] Salt hydrate, inorganic compounds, and metallics are part of inorganic PCMs.

2.2.1 | Salt hydrates

Salt hydrate is an inorganic salt comprising water molecules with a chemical formula of $AB{\cdot}nH_2O$, where AB refers to inorganic salts. The melting and freezing process of salt hydrate is based on the dehydration of hydrated salt. One of the major deprivations of salt hydrate PCMs is incongruent melting, which happens when the salt is not completely soluble in its hydration water at the melting point.[37] Another limitation of this type of PCM is sub-cooling, which may be overcome by encapsulating the PCMs or by adding thickening agents.[24]

Despite these drawbacks, salt hydrates have been used for heat storage applications due to their large energy density, high latent heat, high thermal conductivity, and relatively low cost.[37] Table 3 summarizes the thermophysical properties of the available medium- and high-melting salt hydrate PCMs.

2.2.2 | Inorganic compounds

Inorganic compounds have relatively high melting temperatures and latent heat capacity but are hazardous to the environment and human health.[51] A few inorganic compounds of high-melting temperature PCMs are shown in Table 4.

2.2.3 | Metallics

Metals consist of atomic structures held together by robust metallic bonds, which allow large amount of energy during phase transition. This type of PCM is also known due to its high thermal conductivity, which will improve significantly the heat transfer. In addition, metallics are generally regarded as promising PCM for high-temperature applications due to their high melting point, high heat of fusion per unit volume, following physical and chemical stability.[37] Unfortunately, metallic PCMs are less attractive due to their corrosiveness and heaviness. Table 5 shows the thermophysical properties of metallic PCMs.

2.3 | Eutectic PCMs

Eutectics PCMs are generally obtained from minimum-melting composition of two or more components, each of

TABLE 3 Thermophysical properties of salt hydrate PCMs

Type of PCM	Chemical formula	T_m (°C)	Latent heat (kJ/kg)	Thermal conductivity (W/m.K)	Density (kg/m^3)	Reference
E 83	n.a	83	152	0.62 (s)	NA	49
Aluminium sulphate 18-hoursydrate	$Al_2(SO_4)_3{\cdot}18H_2O$	88	218	NA	NA	8
TH 89		89	149	NA	NA	49
Strontium hydroxide octahydrate	$Sr(OH)_2{\cdot}8H_2O$	89	370	NA	NA	8
Magnesium nitrate hexahydrate	$Mg(NO_3)_2{\cdot}6H_2O$	89.9	167	0.611 (s), 0.49 (l)	1636(s), 1550 (l)	8,37
SP 90		90	150	0.6	1650 (s)	49
Aluminium potassium sulphate dodecahydrate	$KAl(SO_4)_2{\cdot}12H_2O$	91	184	NA	NA	37
Ammonium alum	$(NH_4)Al(SO_4){\cdot}6H_2O$	95	269	NA	NA	50
Lithium chloride monohydrate	$LiCl{\cdot}H_2O$	99	212	NA	NA	8
Magnesium chloride hexahydrate	$MgCl_2{\cdot}6H_2O$	117	167	0.704 (s), 0.57 (l)	1570 (s), 1450 (l)	50
E 117		117	169	0.7	NA	49

TABLE 4 Thermophysical properties of inorganic compound PCMs

Inorganic compound PCMs	Chemical formula	T_m (°C)	Latent heat (kJ/kg)	Thermal conductivity (W/(m K)	Reference
Lithium nitrate	$LiNO_3$	254	360	0.6527	52,53
Sodium nitrate	$NaNO_3$	307	172 to 266	0.561	8
Potassium nitrate	KNO_3	333 to 380	116 to 266	0.4593	8
Potassium hydroxide	KOH	380	149	NA	8
Magnesium chloride	$MgCl_2$	714	452	1.6781	52,53
Sodium chloride	NaCl	800	492	1.0199	52,53
Potassium fluoride	KF	857	452	NA	53
Potassium carbonate	K_2CO_3	897	236	NA	53
Sodium sulphate	Na_2SO_4	901.57	182.3	NA	12

TABLE 5 Thermophysical properties of metallic PCMs

Type of PCM	T_m (°C)	Latent heat (kJ/kg)	Specific heat capacity (kJ/kg K)	Thermal conductivity (W/m K)	Density (kg/m^3)	Reference
$Bi_{52}Pb_{30}Sn_{18}$	96	34.7	0.167	24	9600	54
Sodium	97.83	113.23	1.38	86.9	926.9	54
Bi-Pb	125	NA	NA	NA	NA	37
$Bi_{58}Sn_{42}$	138	44.8	0.201	19	8560	54
Indium	156.8	28.59	0.23	36.4	7030	54
Lithium	186	433.78	4.389	41.3	515	54
$Sn_{91}Zn_9$	199	32.5	0.272	61	7270	54
Tin	232	60.5	0.221	15.08	730	54
Bismuth	271.4	53.3	0.122	8.1	979	54

which melts and freezes congruently, forming a mixture of the component crystals during crystallization.[37] The compositions can be organic-organic, inorganic-inorganic, or inorganic-organic. The melting temperature of composites can be adjusted to a certain point by carrying out different proportion of each element. For instance, the combination of Li_2CO_3 and K_2CO_3 at the weight percentages of 28%:72% and 35%:65% result in melting point at 498 and 505 K, respectively. The combination will therefore provide the benefit of achieving a certain melting point. Thermophysical properties of high melting eutectic PCM are exhibited in Table 6.

2.4 | Comparison of PCMs

Most PCMs are generally characterized by their high latent heat within a wide range of temperatures. Each type of PCMs has its own properties, strengths, and limitations. For instance, low thermal conductivity and flammability in the case of paraffin PCMs. Despite the superiority of salt-based PCM over paraffin in terms of thermal conductivity, they are limited by the incongruent melting, phase segregation, and sub-cooling behaviour. Metallic PCMs possess high melting temperature and high thermal conductivity; nevertheless, corrosiveness restricts their usage. Eutectic PCMs are recognized by their adjustable melting temperature. However, the combination of element to produce eutectic PCM is less attractive due to economic concern.[49]

To overcome the aforementioned shortcomings, improvements are introduced either to reduce those disadvantages or to achieve good performance of PCMs applications. For instance, the integration of PCMs with additives enhances their thermal conductivity and mitigates the flammability of paraffin. Mixing PCMs with nucleating agents is considered one of the ways to diminish sub-cooling of salt hydrate PCMs.

TABLE 6 Thermophysical properties of eutectic PCMs

Type of PCM	Proportions (wt%)	T_m (°C)	Latent heat of fusion (kJ/kg)	Thermal conductivity (W/m K)	Density (kg/m^3)	Reference
$LiNO_3 + NH_4NO_3 + NaNO_3$	25:65: 10	80.5	113	NA	NA	37
$LiNO_3 + NH_4NO_3 + KNO_3$	26.4:58.7:14.9	81.5	116	NA	NA	37
$LiNO_3 + NH_4NO_3 + NH_4Cl$	27:68: 5	81.6	108	NA	NA	37
$AlCl_3 + NaCl + KCl$	60:26: 14	93	213	NA	NA	8
$AlCl_3 + NaCl$	66:34	93	201	NA	NA	8
$KNO_3 + LiNO_3$	67:33	133	170	NA	NA	53
$NaNO_3 + KNO_3$	50:50	220	110.7	0.56	1920	17
$NaNO_3 + KNO_3$	46:54	222	100	NA	NA	53
$KCl + ZnCl_2$	68.1:31.9	235	198	0.8	2480	17
$LiCl + LiOH$	37:67	262	485	1.10	1550	17
$Na_2CO_3 + NaOH+NaCl$	6.4:85.8:7.8	282	316	NA	NA	55
$Na_2CO_3 + NaOH$	17.1:82.9	286	252	NA	NA	56
$NaCl + KCl$	58:42	360	119	0.48	2084.4	17
$Li_2CO_3 + K_2CO_3 + Na_2CO_3$	32.1:34.5:33.4	397	276	NA	NA	55
$MgCl_2 + NaCl$	38.5:61.5	435	351	NA	2480	17
$Li_2CO_3 + K_2CO_3$	46.6:53.4	488	391	NA	NA	55
$Na_2CO_3 + Li_2CO_3$	56:44	496	370	2.09	2320	17
$Li_2CO_3 + K_2CO_3$	28:72	498	263	NA	NA	55
$Li_2CO_3 + K_2CO_3$	28.5:71.5	498	316	NA	NA	55
$Li_2CO_3 + K_2CO_3$	35:65	505	344	NA	NA	55
$NaBr + NaF + Na_2MoO_4$	43:2:55	506	241	NA	NA	55
$K_2CO_3 + NaF + KCl$	62:17:21	520	274	NA	NA	55
$K_2CO_3 + KCl + KF$	37:40:23	528	283	NA	NA	55
$Li_2SO_4 + Li_2MoO_4 + CaMoO_4$	59.8:36:3.5	538	406	NA	NA	55
$Li_2CO_3 + Na_2CO_3 + K_2CO_3$	20:60:20	550	283	NA	NA	55
$Li_2CO_3 + Na_2CO_3 + K_2CO_3$	22:16:62	550	288	NA	NA	55
$KBr + KF$	60:40	576	315	NA	NA	55
$KBr + K_2MoO_4$	65:35	625	90.5	NA	NA	55
$Cu + Ge$	60:40	644	232.8	15	7490	57
$NaF + MgF_2$	75:25	650	860	1.15	2820	17
$Cu + Ge$	50:50	705	198.2	NA	7250	57
$K_2CO_3 + Na_2CO_3$	50:50	710	163	NA	NA	55
$K_2CO_3 + Na2CO3$	51:49	710	163	NA	NA	55
$LiF + CaF_2$	80.5:19.5	767	816	1.7 (s), 3.8 (l)	2390	17
$Cu + Ge$	40:60	765	163.5	NA	7030	57
$NaCl + CaCl_2$	52:48 (mol%)	779.35	164.2	0.704	NA	58

Encapsulation technology has been developed to protect their structural and thermophysical properties. In addition, modification of chemical composition is promoted to ease phase separation in salt-based PCMs. The comparison and improvement methods of various PCMs are shown in Table 7.

3 | MICROENCAPSULATION OF MEDIUM AND HIGH-MELTING TEMPERATURE PCMS

Encapsulation is a coating process of solid, liquid droplets, or gases in a thin continuous polymeric material.[60]

TABLE 7 Comparison of medium and high-melting PCMs

	Organic				Inorganic			
		Non-paraffin						
	Paraffin	Fatty acid	Glycols	Sugar alcohol	Salt hydrate	Inorganic compounds	Metallics	Eutectics
Formula	C_nH_{2n+2}	$CH_3(CH_2)_{2n}.COOH$	(—O—CH_2—CH_2—) with ending groups of (—OH).	—	AB· nH_2O	—	—	—
Latent heat (kJ/kg)	60 to 269[8,31-34,36,49]	125 to 250[49]	—	109 to 294[38]	86 to 328[8,33,34,37,49,50]	10 to 333[38]	11.4 to 433.78[37,54]	95 to 265[8,34,37,49,50]
Thermal conductivity (W/m.K)	0.14 to 0.7 (mostly ~0.02)[8,31-34,36,49]	0.162 to 1.188 (mostly ~0.02)[33,36,37]			0.5 to 1.255 (mostly ~0.07)[8,33,34,37,49,50]	—	8.1 to 86.9[37,54]	0.136 to 0.678[8,34,37,49,50]
Density (kg/m^3)	770 to 1200[8,31-34,36,49]	878 to 1004[49]	—	838 to 1580[38]	830 to 2070[8,33,34,37,49,50]	—	515 to 13 546[37,54]	1440 to 1640[8,34,37,49,50]
Characteristics	Melting temperature relates to the length of the carbon chain	Melting temperature relates to the length of the molecule[33]	Biodegradable[28]	Hydrogenated form of a carbohydrate[33]	Alloys of inorganic salt and water	Relatively low latent heat capacity[8]	Unconsiderable due to weight penalties[37]	Composition of two or more PCMs that melts and crystalizes simultaneously[38]
	The most commercially PCM[49]	Potential materials for future sustainable heat storage products[34]			Phase transition is based on the dehydration of PCMs[37]			
					One of the most used and most studied[38]			
Advantages	High latent heat of fusion	High latent heat of fusion[34,49]			High latent heat of fusion per unit volume[37,38]		High thermal conductivity	No phase segregation[38,49]
	Non-corrosive	Stable upon cycling; No phase separation[33,34]			Considerable volumetric storage density[49,59]		High heat of fusion per unit volume	Good thermal conductivity
	Non-toxic	Mostly are non-toxic[34]			High thermal conductivity[37,38]		Relatively low vapour pressure[37]	
	Chemical stable	Chemical stable[34]			Low price compared with organic PCMs			
	No tendency to supercooling[33,49]	No tendency to supercooling[33,34]			Non-flammable[59]			
		The largest category of PCM[37]			Inexpensive[38,59]			

TABLE 7 (Continued)

	Organic				Inorganic			
		Non-paraffin						
	Paraffin	Fatty acid	Glycols	Sugar alcohol	Salt hydrate	Inorganic compounds	Metallics	Eutectics
	Congruently melting and solidification[33]							
	Varied range of phase transition temperature[49]	Relatively low vapour pressure[28]			Non-corrosive[37]			
	Inert to metal containers[49]							
	Low vapour pressure[33]							
	Good storage density[33]							
Disadvantages	Low thermal conductivity	Low thermal conductivity[33,34,38]			Incongruent melting	Low latent heat of fusion	Low latent heat of fusion per unit weight[37]	Low heat of fusion per unit weight
	Flammability	Flammability[34]			Phase separation	Toxicity	Corrosive	High cost[38,49]
	Incompatibility with plastic containers[33]	Mild corrosive[34]			Supercooling		High cost	
	Relatively expensive[33,34]	Higher cost than paraffin[36,38]					Low specific heat	
							Low specific heat capacity	
Improvement method	High thermal conductivity additives[49,59]	High thermal conductivity additives[49,59]			The introduction of nucleating and thickening agents[37,49,59]			
	Fire-retardant additives[49,59]	Fire-retardant additives[49,59]			Thin horizontal layer arrangement[49,59]			
	The integration with fins for heat transfer enhancement[49]				Mechanical stir[49,59]			
					The use of gel or thickened mixtures			

(Continues)

TABLE 7 (Continued)

Organic				Inorganic			
	Non-paraffin				Inorganic compounds		
Paraffin	Fatty acid	Glycols	Sugar alcohol	Salt hydrate	Metallics	Eutectics	
				eliminate segregation[38]			
				Encapsulating the PCM to reduce separation[37]			
				Modification of chemical composition to achieve congruent material[37]			

The encapsulated substance is referred as the core, while the encapsulating element is called shell or capsule material. Based on their sizes, encapsulation is classified as macrocapsule with a diameter larger than 1 mm, microcapsule in the range between 1 μm and 1 mm, and nanocapsule with a diameter less than 1 μm. In general, microencapsulation techniques are categorized as chemical and physical methods. Chemical microencaspulation method includes in situ polymerization; while sol-gel, spray drying, fluidized bed, and electrohydronamics are extensively used as physical methods to encapsulate the medium and high melting temperature of PCMs. Boehmite treatment followed by heat oxidation is also found recently to encapsulate metal and alloy in Al_2O_3 shell.

3.1 | In situ polymerization

The microencapsulation of PCMs is accomplished chemically by in situ methods such as emulsion, suspension, precipitation or dispersion polymerization, and interfacial polycondensations.[61] In situ polymerization is based on mixing monomers or prepolymers within immiscible liquids of oil and aqueous phase to establish polymerization. Basically, in situ polymerization involves[8]: (a) dispersion of PCM in water as oil in water (O/W) emulsion, (b) prepolymer preparation by mixing different monomers, (c) initiation of the polymerization process by stirring the prepolymer within O/W solution, (d) stabilization of the polymer structure by washing and drying the MEPCM. Emulsion and interfacial polycondensations are commonly used to microencapsulate medium and high-melting PCMs.

3.1.1 | Emulsion/miniemulsion polymerization

The emulsion polymerization method involves combining the monomer with a surfactant in an oil system. The initiator is used to start the chemical reaction and is dissolved in water system, while the monomer is emulsified with the help of a surfactant in the polymerization medium. Because the initiator is only present in the aqueous phase, the polymerization reaction begins in this phase (ie, outside of the droplets and micelles) and subsequently progresses to the micelles.[62] The method of miniemulsion polymerization is similar to that of emulsion polymerization, with the exception that smaller droplets can be generated using high-shear devices such as ultrasound and high-pressure homogenizers.[61]

Şahan et al[40] investigated the nanoencapsulation of stearic acid (SA) with melting temperature about 66°C to

83°C using polymethyl methacrylate (PMMA) (SA0) and four PMMA-hybrid shell structures. The PMMA-hybrid shells were synthesized using different reagents, such as methyacrylate (SA1), 2-hydroxy-ethylacrylate (SA2), silica (SA3), and styrene (SA4). Differential scanning calorimetry (DSC) test resulted in melting temperature of MEPCMs were in the range of 60°C to 89°C with the maximum encapsulation efficiency by about 38.9% for SA1, as summarized in Table 8. Thermal stability of all microcapsules was compared with SA and it exhibited an increase in the core material's thermal degradation temperatures in all microcapsules, demonstrating that encapsulation can improve SA's thermal stability. Scanning electron microscope (SEM) images show that the PMMA-HEA (SA2) was the most spherical of the five varieties created, while the PMMA-SiO_2 shell (SA3) had irregular shapes. They concluded that water solubility and interfacial tension variations between core and shell were the most important chemical variables that dictated the preferred morphology. The authors suggested that SA2 and SA4 be investigated further.

Fuensanta et al[14] adopted miniemulsion polymerization to encapsulate RT80 paraffin ($T_m = 85.1°C$) in a a styrene-butyl acrylate (SBA) copolymer shell. Sodium dodecyl sulphate (SDS) was selected as surfactant, and various surfactant/paraffin mass ratios were investigated. The presence of RT80 in the nanoencapsulated PCM (nPCM) was confirmed by Fourier transform infrared (FT-IR) spectra exhibiting typical bands of both the RT80 and the shell employed to create the nPCM. According to the nPCM size study, the amount of SDS in the particle size was more noticeable when using less RT80. This was supported by the morphology of the nPCM observed by SEM . With increasing SDS, the particle size of the nPCM obtained with the same mass content of the RT 80 dropped marginally. The melting and crystallization heat of nPCM were found about 10 to 20 J/g with reduction of 87.6% to 93.8% when compared with pristine RT80, according to DSC results. After 200 thermal cycles, the nPCM's thermal stability was confirmed by a minor change in thermal characteristics. The TGA was used to assess the thermal stability, and results showed that nPCM had a higher temperature degradation than raw RT80, indicating that it had a stronger thermal stability.

The emulsion polymerization of inorganic PCMs could be accomplished in two ways: either by generating an oil in a water system (O/W) emulsion for direct emulsion, or by producing water in an oil system (W/O) emulsion (inverse emulsion). For instance, Graham et al[63] demonstrated the nanoencapsulation of magnesium nitrate hexahydrate ($Mg[NO_3]_2.6H_2O$) by employing in situ inverse miniemulsion polymerization with poly(ethyl-2-cyanoacrylate) (PECA) shell material. The W/O emulsions were prepared using toluene and cyclohexane as oil phase, while the aqueous phase consisted of different PCM/water ratios. Ethyl-2-cyanoacrylate (ECA) was employed as a monomer and subsequently added to the W/O mixture dropwise at different volume. Two samples of nanoencapsulated PCMs (NanoPCM), NanoPCM1 and NanoPCM2, were fabricated using toluene as the oil phase with a different ratio of aqueous phase, while NanoPCM3 was prepared using cyclohexane with less surfactant and followed by ultrasonic treatment prior to the addition of ECA. It was obtained that all NanoPCMs were well encapsulated with smooth surface. Furthermore, after heating to 800°C, the TGA exhibited that NanoPCM3 had more $Mg(NO_3)_2{\cdot}6H_2O$ than NanoPCM1 or NanoPCM2. The DSC results indicated that the highest encapsulation efficiency was achieved by NanoPCM3 by about 51.93% with a melting point and latent heat by about 91°C and 83.2 J/g, respectively, which remained almost constant after 100 cycles. Another interesting finding was that the NanoPCM3 considerably reduced supercooling and phase separation during heating and cooling without damaging the capsule shell.

Furthermore, Graham et al[64] encapsulated $Mg(NO_3)_2{\cdot}6H_2O$ and sodium sulphate decahydrate ($Na_2SO_4{\cdot}10H_2O$, $T_m = 32°C, \Delta h_m = 228.1\,J/g$) using PECA shell material as NanoPCM1 and NanoPCM2, respectively. Moreover, NanoPCM3 and NanoPCM4 capsules were sequentially prepared containing the mixture of $Mg(NO_3)_2{\cdot}6H_2O$ and $Na_2SO_4{\cdot}10H_2O$ with the weight ratio of 1:1 and 1:2. The encapsulation was carried out by in situ inverse miniemulsion polymerization combined

TABLE 8 DSC and TGA results of stearic acid (SA) with PMMA and four PMMA-hybrid shell structures[40]

	SA	SA0	SA1	SA2	SA3	SA4
Melting temperature (°C)	66 to 83	64 to 84	66 to 86	65 to 89	64 to 89	60 to 85
Storage capacity (J/g)	189	50	73.5	70.8	60.4	63.3
Encapsulation percentage (%)	—	26.5	38.9	37.5	32	33.5
On-set PCM mass loss (°C)	160	160	160	160	150	160
Degradation temperature (°C)	226	340	325	340	290	347

Note: Reused with permission from Elsevier license number 5193620427763.

with ultrasonic treatment. Results showed that the diameter of NanoPCMs was in the range of 100-300 nm with the smooth PECA shell through SEM images. TGA curve was used to observe the reduction of water loss in NanoPCM2, NanoPCM3, and NanoPCM4 as the increase of $Na_2SO_4{\cdot}10H_2O$ content in the capsules. This study also investigated two types of mixture: (a) single NanoPCM1 and NanoPCM2 in different ratios, and (b) NanoPCM3 and NanoPCM4 capsules containing the mixture of salt hydrate PCMs as core component. The DSC results showed the multiple melting points of the NanoPCM mixture in Figure 2C,D which was attributed to the phase transition of each PCM with maximum latent heat reduction of about 80% to 83%. Meanwhile, the transition temperature of NanoPCM3 (Figure 2E) was unstable and they found it difficult to predict the latent heat. In contrast, the phase transition of NanoPCM4 in Figure 2F was clearly shown at melting point of 15.4°C in 67% encapsulation efficiency with the supercooling reduction of 16.5°C.

3.1.2 | Interfacial polymerization

The interfacial polymerization is characterized by the formation of polymerization at the surface of dispersed PCM as core material. The interfacial polymerization is based on the dissolution of oil-soluble reactive monomer in the organic phase consisting of core materials, followed by the introduction of water-soluble reactive monomer into the dissolution prior to polymer shell formation.

Hayashi et al[65] adopted interfacial polymerization to encapsulate erythritol in polyurethane shell material. Polyethyleneglycol (PEG) 600 was selected as water-soluble monomer and subsequently mixed with erythitol to be dissolved in distilled water to prepare the aqueous phase. The solution was then added to corn oil as oil phase to establish W/O emulsion. Three different isocyanate monomers (toluene diisocyanate [TDI], diphenyl methane diisocyanate [MDI], and hexamethylenediisocyanate [HDI]) were employed as oil-soluble monomer. The isocyanate was mixed afterward to W/O emulsion to form polymer shell material, and it was observed the rough surface of each sample through SEM images. They also reported that microencapsulation using TDI, MDI, and HDI achieved maximum encapsulation efficiency respectively, about 82%, 50%, and 40%. The DSC results showed that microcapsules prepared with TDI achieved the highest latent heat, about 82 J/g, without any significant change of melting temperature at 121°C. The MEPCM using TDI was subsequently investigated to study the effect of supercooling prevention agent by employing potassium dihydrogen phosphate and

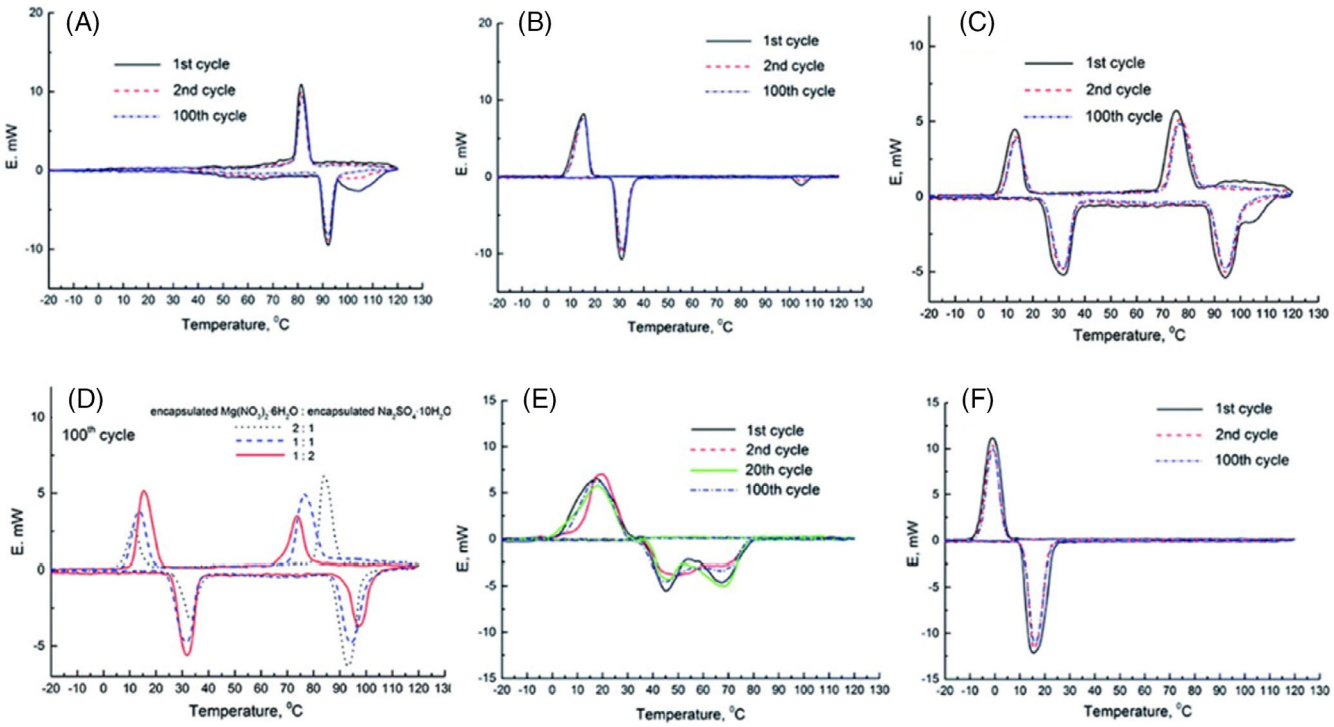

FIGURE 2 DSC for (A) NanoPCM1, (B) NanoPCM2, (C) 1:1 NanoPCM1:NanoPCM2 ratio, (D) different NanoPCM1: NanoPCM2 ratio, (E) NanoPCM3 (encapsulated 1:1 wt% $Mg(NO_3)_2.6H_2O$: $Na_2SO_4{\cdot}10H_2O$), (F) NanoPCM4 (encapsulated 1:2 wt% $Mg(NO_3)_2{\cdot}6H_2O$: $Na_2SO_4{\cdot}10H_2O$). Reused from Graham et al[64] with permission from The Royal Society of Chemistry

calcium sulphate with PCM. Results revealed that the crystallization temperature of PCM shifted from 21°C to 100°C due to the introduction of supercooling prevention agent.

3.2 | Sol-gel encapsulation

Sol-gel method is defined as the production of an oxide association in a liquid via polycondensation reactions of a molecular precursor. The sol-gel encapsulation process is initiated by uniformly mixing of precursor in liquid phase followed by the hydrolysis condensation chemical reaction to generate a stable dispersion of colloidal solution (sol) particles. A gel with a three-dimensional network structure is subsequently formed by the assembly of the sol.[61]

In this technique, silicon dioxide (SiO_2) is typically utilized as the shell material, which has thermal stability, mechanical strength, and can withstand high temperatures.[66] Tetraethylorthosilicate (TEOS) is employed by many studies as precursor, and the appearance of silica nuclei via hydrolysis and condensation of TEOS is described as follows[12]:

$$\text{Hydrolysis} :: Si(OC_2H_5)_4 + 4H_2O \rightarrow Si(OH)_4 + 4C_2H_5OH$$

$$\text{Condensation} : Si(OH)_4 + (OH)_4Si \rightarrow \equiv Si - O - Si \equiv + H_2O$$

Microencapsulated $NaNO_3$ was prepared by Sanchez et al[67] by adopting sol-gel method using SiO_2 shell. The SiO_2 precursor was TEOS, with the molar ratios of 1:0.5 and 1:0.25 to PCM, and labelled respectively as Na-0.5Si and Na-0.25Si. According to the SEM images, the $NaNO_3$ in Na-0.5Si had crystallized into bundles with SiO_2 microparticles coated on them in particle size of 0.2 to 0.5 μm. Micrographs of Na-0.25Si, on the other hand, showed prismatic shape $NaNO_3$ crystals coated shell in the range of 0.5 to 1 μm. In addition, DSC result exhibited melting peak at about 306.8°C with enthalpy 158.1 J/g. It was also reported that the presence of SiO_2 caused some discrepancies in the thermal behaviour of synthetized Na-0.5Si and Na-0.25Si microparticles. Due to the presence of SiO_2, the melting points of Na-0.5Si and Na-0.25Si were changed to 294.2°C and 293.4°C, respectively, in accordance with an encapsulation efficiency of 11.43% and 15.74%. After that, the thermal stability of Na-0.25Si was examined, and the results revealed that it was more stable than Na-0.5Si even after 20 thermal cycles with constant melting and cooling enthalpies of 20 and 22 J/g, respectively.

Wu et al[12] prepared microencapsulated composite material using Na_2SO_4 as core and SiO_2 as shell using the sol-gel method. To explore the impacts of silica mass percentages on the thermal properties of MEPCMs, TEOS was utilized as the silica precursor, and various masses of Na_2SO_4 were synthesized with the ratio of 2.7% to 26.8%. SEM images showed that the MEPCM with 5.4% silica added had a homogenous structure throughout the whole Na_2SO_4 particle. Due to the increase of silica mass percentage, specific heat capacity and thermal conductivity increased first and subsequently declined. Because of the limited impact of silica outside, the peak melting temperatures essentially rose with the increase of silica mass percentages, as shown in DSC thermogram. DSC also showed that with silica additions of 2.7% and 3.8%, the latent heat of pure Na_2SO_4 rose from 182.3 to 211.0 J/g and 194.8 J/g, respectively, which might be promoted by the silica phase transition. The MEPCM with 5.4% of silica could be a tipping point for the silica phase transition and the Na_2SO_4 solid-liquid phase transition, resulting in a lower total heat release about 170.6 J/g, than pure Na_2SO_4. The overall heat storage density of 5.4% silica, including latent heat and sensible heat, was 390.6 J/g for working temperatures ranging from 850°C to 950°C, which proved critical for thermal storage applications. Furthermore, they discovered that after 50 thermal cycle tests, the latent heat loss of MEPCM with 5.4% silica was just 4.3%, which was finally determined as the best sample in this study.

Zhang et al[66] investigated the microencapsulation of KNO_3 in silica shell for high-temperature applications of more than 300°C. The capsules were obtained by employing different amount of TEOS from 0.5 to 2 mL. It was observed the rougher surface morphology of silica shell as the increase of TEOS concentration. They assumed that the smoother shell development was due to the smaller primary silica nuclei size and lower silica condensation degree. DSC was utilized to describe the phase change behaviour of the MEPCMs, as well as to investigate the sample's heat storage capability and thermal stability. The greatest encapsulation efficiency was determined to be around 98.8% for 0.5 mL of TEOS. All other MEPCMs with lower encapsulation ratios, on the other hand, were found intact after 10 cycles of DSC testing. They concluded that the MEPCM with 0.75 mL TEOS exhibited a stable shell after durability testing and a high encapsulation ratio of 95.2%.

Moreover, the microencapsulation for binary carbonate salt of Li_2CO_3 and Na_2CO_3 in silica shell was developed by Zhang et al[68] through water-limited sol-gel method with TEOS as precursor. By restricting the amount of water in the solution, binary salt may exist as a solid particle on which the silica might cover. TEOS concentrations of 1.5 and 2 mL were used during the preparation and were denoted respectively as LiNa@Si-

1.5 and LiNa@Si-2. DSC test was carried out to show the 498.6°C of melting point with latent heat of 360.5 J/g. Besides that, LiNa@Si-1.5 had a latent heat of 250.9 J/g and a melting point of 498.6 C, resulting in an encapsulation ratio of 69.6%. Because of the greater silica concentration in LiNa@Si-2, it could only regain a latent heat of 131.3 J/g. It was also found that after 100 cycles, 82% of the latent heat by around 220.7 J/g could be preserved at 494.3°C of melting point. Another significant discovery was that LiNa@Si-1.5 had a considerably greater effective heat capacity of around 516 J/g for temperatures ranging from 400 C to 540 C, an increase of 134.4% above binary salt.

He et al[69] selected Al-Si eutectic PCM and synthesized Al_2O_3 as shell material using aluminium precursor. The microencapsulation was performed in sol-gel process and the developed MEPCMs were investigated for multiple thermal cycling. The SEM micrographs of MEPCM after multiple heat cycles are presented in Figure 3. The initial surface of MEPCMs in Figure 3A was smooth and thick, with no defects or cracks, and was remarkably comparable to the five heat cycles depicted in Figure 3B. The MEPCMs after 15 cycles (Figure 3D) also had an incorporated spherical particle; however, it began to lose its smooth surface and transformed to a fractured morphology due to excessive sintering, which caused some of the gel pieces to flake. Regardless of surface shape, the thermal stress caused by solid-liquid cyclic phase transition did not fully disintegrate the shell after 15 cycles. According to the TG curve, when the shells of MEPCM cracked during the thermal cycling process, the majority of samples showed a similar pattern of mass increase, which was primarily driven by oxidation of the exposed Al-Si alloy core. This phenomenon was also shown during DSC test with a mass increase of about 0.35% to 3.77%. The DSC findings also indicated the reduced latent heats during thermal cycling, from 307.21 kJ/kg of MECPM to 271.90 kJ/kg of MEPCM after 20 cycles. The link between cracked ratio and thermal cycling times was also investigated, with findings revealing that the cumulative cracked ratio surpassed 20% at the 20th time cycling.

3.3 | Spray drying

Spray drying involves dispersing the PCM in aqueous coating solutions to produce the desired size of microcapsules. The liquid emulsion is then atomized into droplets. The water is subsequently evaporated in a drying chamber, allowing the active components to be encased in an encapsulating material matrix. The schematic diagram of spraying drying method is illustrated in Figure 4. The benefits of spray drying include cheaper manufacturing costs, higher yields, less waste of raw materials, ease of control, and multi-purpose applications. The primary disadvantages of this technique, on the other hand, are agglomeration and the fact that leftover particles are not encapsulated.[70]

Tudor et al[53] selected potassium nitrate (KNO_3) with melting and crystallization point of 338.5°C and 319.1°C, respectively, into an inorganic shell of ZnO. Solvothermal technology and spray drying were carried out for microencapsulation process at various weight ratios of ZnO:

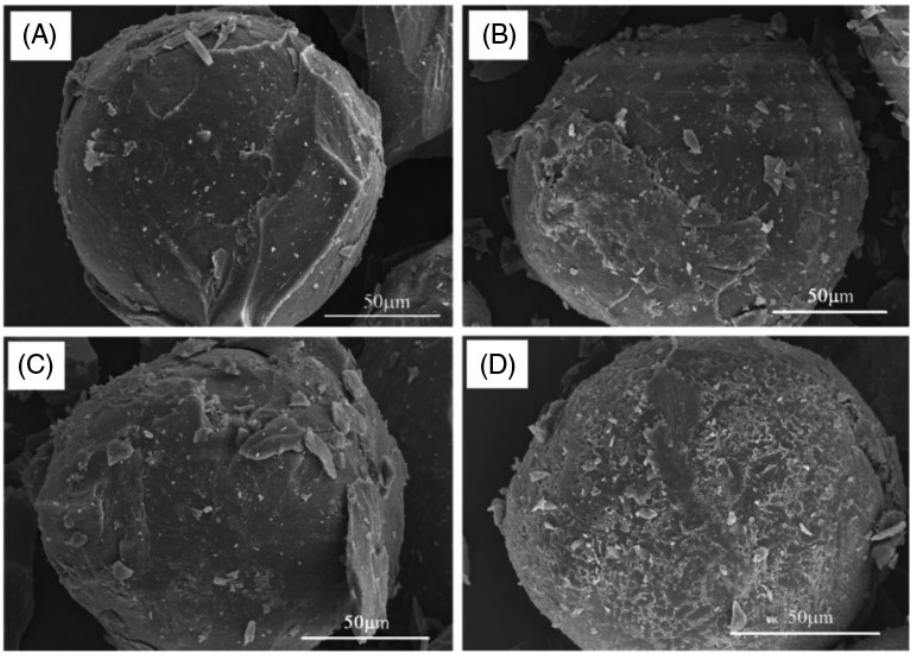

FIGURE 3 SEM images of MEPCM after (A) 0, (B) 5, (C) 10, (D) 15 thermal cycles.[69] Reused with permission from Elsevier license number 5260831069677

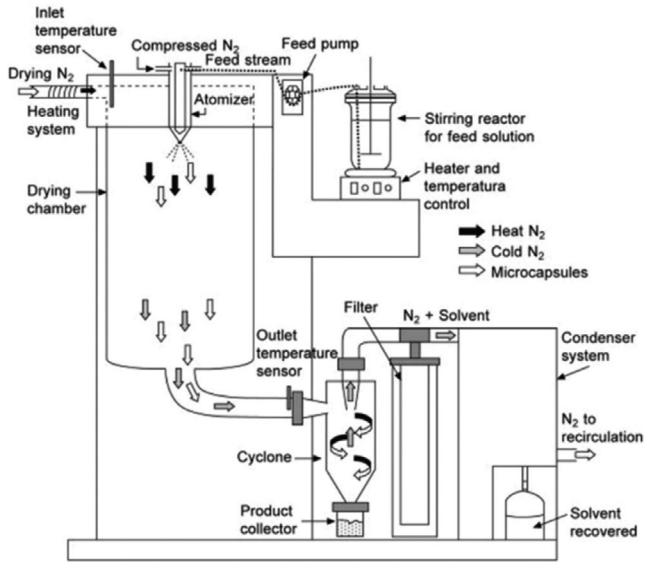

FIGURE 4 Schematic of MEPCM fabrication through spray drying.[60] Reused with permission from Elsevier license number 5260841023950

KNO_3 in the range of 1:1 to 1:5 with different synthesis temperatures. Aside from KNO_3 and ZnO, secondary zinc nitrate hydroxide hydrate ($Zn_5(OH)_8(NO_3)_2(H_2O)_2$) was discovered during the manufacturing at synthesis temperature below 200°C. According to DSC findings, the melting/crystallization temperatures of MEPCM with the weight ratio of 1:5 were slightly lower than those of pure KNO_3, 328.5°C/312.6°C and 336.1°C/323.7°C, respectively, in agreement with synthesis temperatures below and above 200°C. Meanwhile, the latent heat of samples synthesized at temperatures lower than 200°C was almost half than that of those synthesized at temperatures higher than 200°C. This finding was explained due to the presence of $Zn_5(OH)_8(NO_3)_2(H_2O)_2$ phase. However, thermal stability was not covered in this study.

Furthermore, Romero-Sachez et al[71] microencapsulated KNO_3 with ZnO shell by the same method as in Reference 53. The samples were prepared at various KNO_3/ZnO mass ratios and different temperatures in solvothermal process. The KNO_3-ZnO P2 and P4 represented the samples with the 3:1 KNO_3/ZnO mass ratio in synthesis temperature of 110°C and 200°C, respectively. Meanwhile, KNO_3-ZnO P3 and P1 denoted the microcapsules with a 5:1 KNO_3/ZnO mass ratio and a synthesis temperature of 200°C and 110°C, respectively. The samples KNO_3-ZnO P2, P3 and P4 were observed in SEM images and it was shown that P2 sample resulted in ZnO microparticles with varying morphologies, including spherical and urchin-like forms, which was attributed to the intermediate zinc hydroxide compound. In addition, the temperature increase during solvothermal process promoted the development of ZnO in spherical shape, which covered the KNO_3 particles in P3 and P4 samples. Another interesting finding showed that DSC curves for both KNO_3-ZnO P2 and P4 revealed two endothermic points at 133.7/139.6°C and 328.3/339.1°C, respectively, which related to pure KNO_3 phase transitions. The thermal stability was further examined for 20 cycles, and it was discovered that the enthalpy rise of KNO_3-ZnO P2 as the increase of cycles number both in melting and crystallization. In contrast, even after 20 heat cycles, the enthalpy of KNO_3-ZnO P4 remained unchanged.

3.4 | Fluidized bed

This encapsulation method is based on the following steps: (a) the atomized shell material is mixed into the fluidized bed particle of PCM, (b) solvent is evaporated while shell material coated the PCM, (c) drying the MEPCM for avoiding agglomeration of solid particles. Figure 5 illustrates the experimental design of this method. A blower is utilized to flow various mass rate of air, and subsequently heated by electrical heaters before entering the column. The uniform distribution of air gets into the plenum of the column before flowing to the bed through a distribution plate.

Fluidized bed was selected by Ushak et al[73] to encapsulate inorganic PCM of $MgCl_2{\cdot}6H_2O$ and Bischofite (95% $MgCl_2{\cdot}6H_2O$). Following compatibility testing, acrylic and chloroform were chosen as the polymer and solvent, respectively. During fluidization production yield, various fluidization time and atomization flow were carried out to achieve maximum yield. The results indicated that a

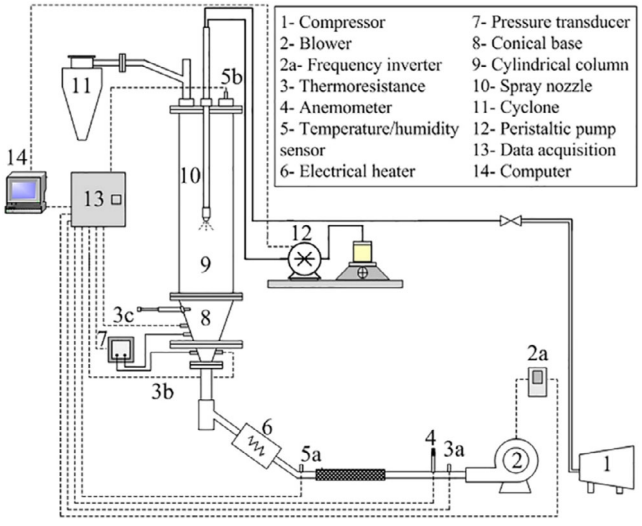

FIGURE 5 Schematic diagrams of fluidized bed.[72] Reused with permission from Elsevier license number 5260841360331

fluidization time of 120 seconds and an atomization flow rate of 2 kg/h were optimal for achieving a maximum yield of encapsulated bischofite and $MgCl_2{\cdot}6H_2O$ of 72.5% and 84.9%, respectively, in accordance with an encapsulation efficiency of 87% and 92%. They reported the melting temperatures for bischofite and $MgCl_2{\cdot}6H_2O$, respectively, as 104.6°C and 95.3°C, which was slightly lower than pure bischofite and $MgCl_2{\cdot}6H_2O$. Unfortunately, the encapsulated inorganic PCMs suffered from the supercooling phenomenon. Visual observation and an optical microscope were used to examine the morphology of the microencapsulated PCM and it was obtained an extremely high encapsulation efficiency through the image of $MgCl_2{\cdot}6H_2O$. This was indicated by the sample being totally red, while the bischofite image revealed blue and white portions representing encapsulated crystals and non-encapsulated crystals.

3.5 | Hydrolysis followed by heat oxidation

Nomura et al[74] developed MEPCM consisting of Al-25 % Si alloy core into α-Al_2O_3 shells using hydrolysis treatment followed by heat oxidation. The technique was based on two steps, as in Figure 6: (a) boehmite treatment for AlOOH preparation shell by hydroxide precipitation process in hot water, and (b) heat-oxidation treatment in an O_2 atmosphere to form stable α-Al_2O_3 shells by heating from room temperature up to 930°C before finally cooled down to room temperature. A fast weight increase in the 530°C to 650°C range and at 705°C of TG was detected as a result of rapid Al oxidation. Cracks appeared on the shell at these points as a result of thermal expansion of the shell material produced by volume expansion of the PCM core. The weight increase appeared to cease around 705°C, indicating the development of a transient stable oxidation coating on the interfacial surface of the exposed liquid Al, which prevented leakage and oxidation of inner liquid Al. The developed MEPCM had a phase transition temperature at 573°C, which was close to that of the pristine PCM, about 577°C. The MEPCM had a latent heat of 247 J/g, which was approximately 57% of the raw material. In addition, after 10 cycles, the MEPCM's phase change temperature and latent heat were fairly similar to those measured during the first cycle, indicating that the MEPCM retained its original structure without leaking.

Furthermore, Nomura et al[75] developed the encapsulation of Al-25 wt% Si microspheres using α-Al_2O_3 shells by employing boehmite and heat-oxidation treatment as in Reference 74. In this study, during heat oxidation, the sample was heated from room temperature to 1130°C prior to finally cooling to room temperature again. The MEPCM in this study were compared with the sample with heat oxidation at 930°C in Reference 74, and they found that the MEPCM had thinner and more continuous bands of crystals as a result of the higher temperature heat-oxidation treatment. DSC result showed the melting and crystallization temperature of MEPCM was respectively 579°C and 530°C, which was comparable with the core's. Meanwhile, the latent heat of the MEPCM was about 54% that of the raw material. The most interesting finding was that the samples achieved almost constant temperature and latent heat after 300 cycles and retained its original structure without leaking. Unfortunately, supercooling remained a concern in that investigation.

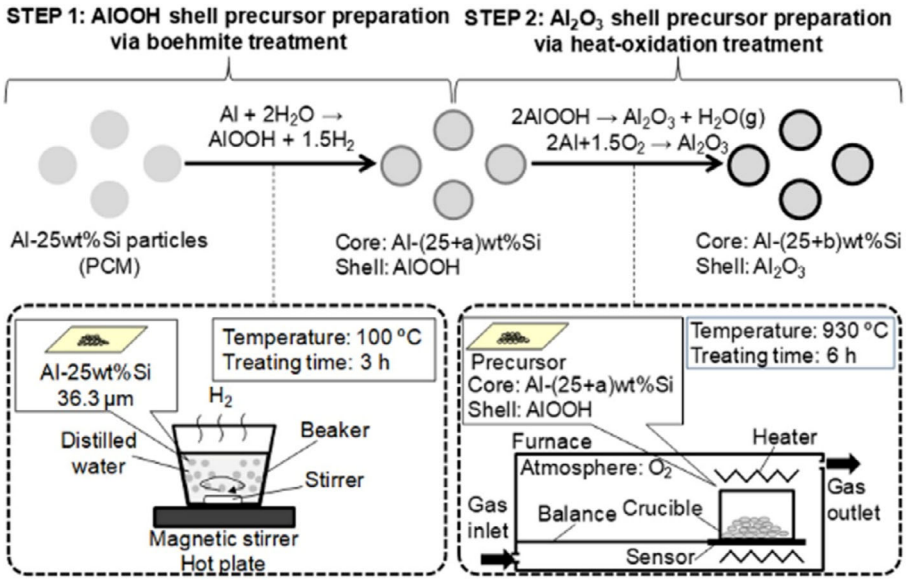

FIGURE 6 Schematic diagram for the preparation of MEPCM. Reused from Nomura et al[74] with permission from Springer Nature

Nomura et al[76] followed the process described in References 74 and 75 for encapsulating Al in Al_2O_3 shells, where heat oxidation treatment was performed at temperatures 1100°C, 1150°C, and 1200°C. The raw Al material was chosen as the core material due to its comparatively high latent heat of 384 J/g at 660°C melting temperature. The DSC results indicated the reduced MEPCMs' heat storage capacity as the rise of heat oxidation temperature. The reductions were around 21.6%, 23.2%, and 28.9%, respectively, for generated MEPCM at 1100°C, 1150°C, and 1200°C heat oxidation temperatures. Meanwhile, the melting point of all MEPCMs remained relatively consistent at 660°C. Additionally, an interesting observation was that MEPCMs with a higher heat oxidation temperature demonstrated superior cyclic endurance after 100 thermal cycles.

Sheng et al[77] modified the microencapsulation method of boehmite and heat-oxidation treatment in Reference 74 to enhance the thermal stability of microencapsulated Al-25% Si alloy and self-repairing Al_2O_3 shell. To offer an additional aluminium source, the boehmite treatment was initially performed in an $Al(OH)_3$ solution with an adjusted pH value prior to precipitation of more $Al(OH)_3$ on the surface. Finally, heat-oxidation treatment at temperature 1150°C was carried out in an O_2 atmosphere. The SEM images of MEPCM samples were observed, and they exhibited a less rough and reasonably compact surface shape when compared with those that had not been treated with precipitation. It was also observed the more stuck of tiny particle on the surface for sample with the addition of $Al(OH)_3$. This finding corresponded to the formation of θ-Al_2O_3, which could increase the shell strength. After 100 thermal cycles, it was obtained that the sample with pH 9 suffered from shell breakage. Thermal stability test was subsequently conducted, and the MEPCMs obtained at pH 8 exhibited less breakage ratio than those of the prepared sample at pH 7. They reported the latent heat of the sample with pH 8 was about 183 J/g, which was lower than the prepared samples in Reference 75 due to the thicker Al_2O_3 shells in this study. Interestingly, the samples obtained at pH 8 achieved high durability until 3000 cycles without obvious leakage or cracks.

Kawaguchi et al[78] modified the MEPCM with Al-based and Al_2O_3 shell. Prior to boehmite treatment, $Al(OH)_3$ was used to modify the coating thickness. The precipitation treatment was subsequently conducted in distilled water at 75°C for 16 hours prior to heat oxidation at 1200°C and 1300°C. The samples were then compared with the fabricated MEPCM in Reference 73, and it was discovered that the modified samples included voids in almost half of the MEPCM particles, which allowed volume expansion during phase change. Due to the existence of voids, it was confirmed that the modified MEPCM demonstrated excellent durability three times than samples in Reference 73, about 300 cycles, with a maximum latent heat capacity of 186 J/g.

Sheng et al[79] synthesized the MEPCM of Al-25 wt% Si with in multilayer of Al_2O_3 and Cu shell for enhancing the thermal performance. Boehmite was initially used to prepare the Al_2O_3 shell precursor, followed by heat treatment and oxidation to prepare the Al_2O_3 shell, prior to HCl etching to improve adhesion. Finally, formation of copper multilayer shell was created by chemical plating process. A high melting temperature of MEPCM by 570°C with an enthalpy of fusion of 100 J/g was achieved. After 100 thermal cycles, the produced MEPCM exhibited two melting points of 518°C and 570°C, respectively, corresponding to enthalpies of 25 and 41 J/g. SEM images showed the retained original MEPCM samples without any leakage and low broken ratio after 10 and 100 cycles, as displayed in Figure 7.

Following the method described in Reference 79, Li et al[80] prepared the microencapsulation of aluminium in the composite shell material of Al_2O_3 and copper. The DSC curves resulted in latent heat decrease due to the formation of multilayer shell of MEPCM. Additionally, after 10 melting-solidification cycles, the latent heat was reduced to 63.46 J/g while the melting point remained nearly constant, which was also characterized by smooth and thick shell surface.

Li et al[10] developed another composite shell material by employing Al-10 wt% Zn alloy as the PCM in composite Al_2O_3, ZnO, and Cu shell materials using the procedure outlined in Reference 79. After copper plating, the latent heat of Al-Zn alloy was lowered by approximately 50%, from 176 to 89 J/g, while the melting temperature was slightly decreased at 638.6°C. The MEPCMs were then subjected to 50 thermal cycles, with the findings indicating a latent heat of approximately 66 J/g without cracks or leakage.

Kawaguchi et al[81] developed the microencapsulation of Zn-30% Al alloy by employing the hydrothermal method followed by heat-oxidation treatment for middle-high temperature applications. The composite consisting of MEPCM and glass frit (GF) as a sintering agent was subsequently prepared at a weight ratio of 1:1. The DSC curves and SEM images were employed to analyse the raw materials, as-prepared MEPCMs, as-prepared composites, and composites after cyclic testing 100 times. DSC results exhibited phase change temperature in the range of 437°C to 512°C for MEPCM and MEPCM-GF composite. Nevertheless, the heat capacity of the as-prepared MEPCMs was decreased from 166 to 117 J/g compared with the raw material. The reduction was attributed to the formation of an oxide coating on the

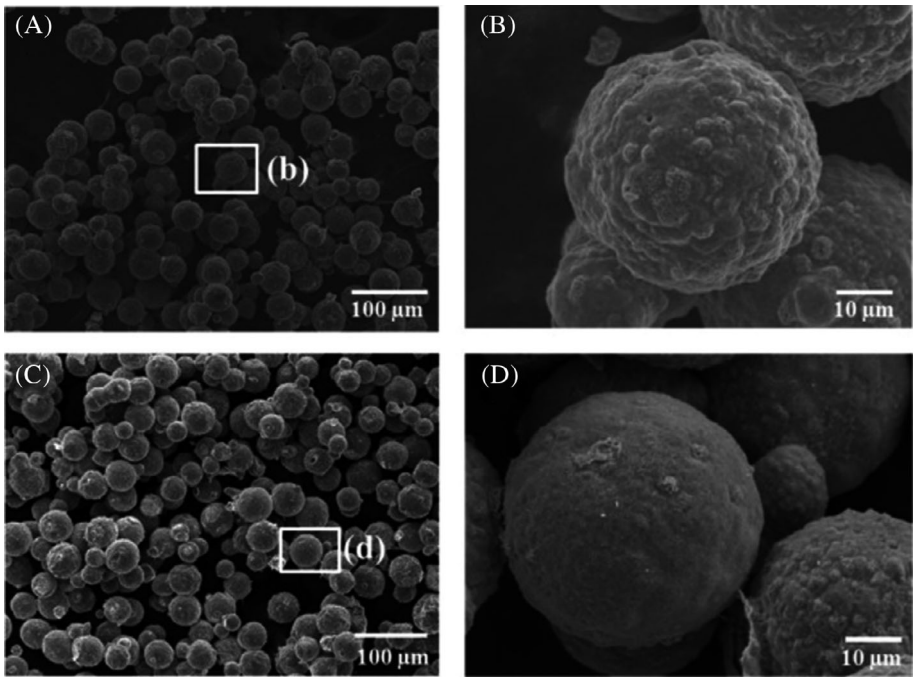

FIGURE 7 SEM images of MEPCM after (A and B) 10 and (C and D) 100 cycles.[79] Reused with permission from Elsevier license number 5260850010440

sample surface. Meanwhile, the heat capacity of the MEPCM-GF composite was 48 J/g and the heat capacity was the same after 100 thermal cycles.

3.6 | Other methods

Other methods, such as solvent extraction, "double-layer coating, sacrificial inner layer," combination of mixing and sintering, etc, exist in addition to the encapsulating technologies.

Li et al[82] prepared the microcapsules made of perhydropolysilazane (PHPS) as the shell material and sodium nitrate ($NaNO_3$) as the core. Microcapsules were prepared through solvent extraction and ultrasonic dispersion. Initially, PHPS solution was entirely mixed with $NaNO_3$ particles. Prior to particle dispersion using an ultrasonic processor, tridecane was added to the solution as an organic solvent. Finally, residual tridecane was filtered out of the produced MEPCM powders. In addition to particle size distribution, SEM images were utilized to show that MEPCM particle sizes of 10 to 300 μm were larger and more uniform than $NaNO_3$ particles. This was generated by tiny $NaNO_3$ particles clumping together to form a larger particle. The DSC thermogram of $NaNO_3$ and MEPCM indicated that MEPCM had a lower latent heat of 159.2 J/g than pure $NaNO_3$ by 188.2 J/g. When compared with $NaNO_3$, the melting and solidification points of MEPCM were 306.19 and 300.44°C, respectively, without significant change of melting point and 3°C reduction of freezing point. TG curve confirmed the 36°C decomposition temperature enhancement of MEPCM compared with the pure PCM. After heating the MEPCM sample up to 350°C, no significant difference in thermophysical properties and morphologies were obtained.

Leng et al[13] microencapsulated binary eutectic salt PCM of NaCl and KCl in a diatomite shell material with different ratios. Before melting at 680°C to create eutectic salt, the NaCl and KCl were thoroughly mixed with a ball mill in a mole ratio of 1.02:1. After cooling down the salt to room temperature, it was crushed and processed to a particle size of 200 to 400 μm in a ball mill. The encapsulation was developed by using a combination of mixing and sintering method. For subsequent usage, the diatomite was crushed down to 3-5 μm particles in a ball mill. A particular amount of water was sprayed on the surface of the eutectic salt powder, and then the diatomite particles were added to obtain final MEPCM. Using a tableting machine, the encapsulated samples were then put into a mould for the pressing process, resulting in green pellets. Afterwards the DSC test was conducted at various weight of PCM and diatomite and displayed as in Figure 8A. The 70% of salt concentration was subsequently investigated according to the highest compressive strength with 393.3 J/g of energy density. Furthermore, the thermal stability of sample was studied, and after 1000 thermal cycling, the melting enthalpy of MEPCMs decreased from 179.3 to 163.1 J/g without any significant change of melting point, as depicted in Figure 8B.

Wei et al[15] prepared the microencapsulation of Al-Si alloy composition and Al_2O_3 shell material. The

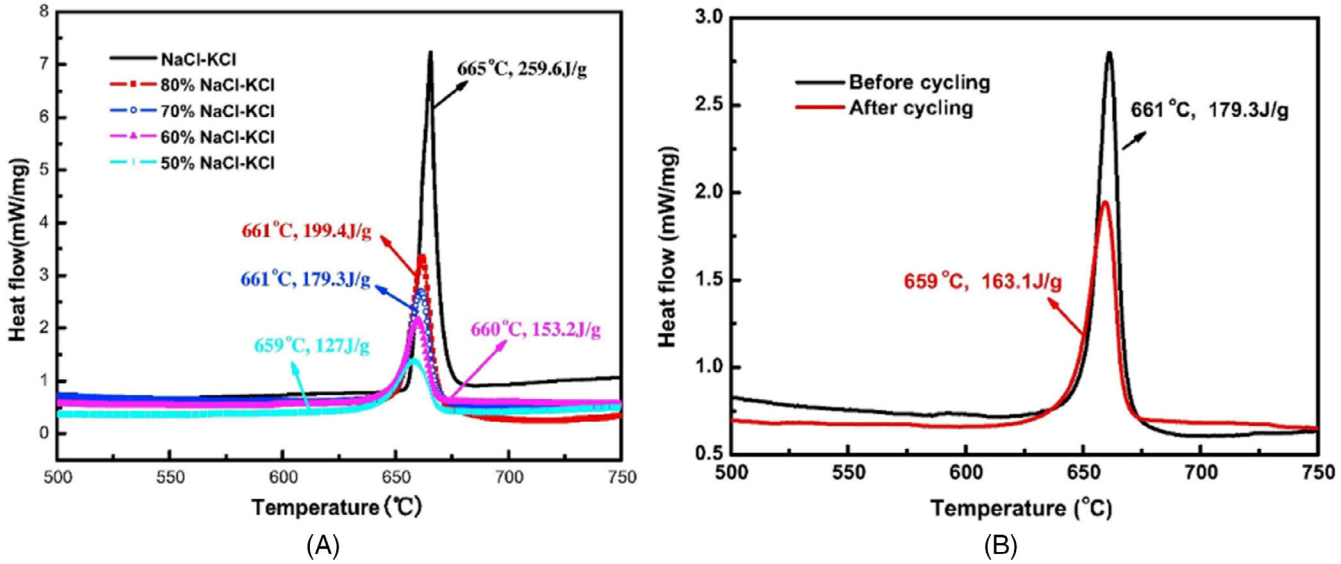

FIGURE 8 DSC thermograms for (A) eutectic sal and different ratios of MEPCM, and (B) MEPCM with 70% salt concentration before and after 1000 thermal cycling.[13] Reused with permission from Elsevier license number 5260850262098

microencapsulation procedure was mainly composed of the formation of a precursor shell on Al microspheres and the subsequent calcination in an argon atmosphere, as displayed in Figure 9. Precursor TEOS was employed in varying compositions from 3.9 until 5.1 g to develop the MEPCMs with tunable melting temperature. DSC resulted in the rise of MEPCMs melting temperature in the range of 574°C to 641.4°C for higher TEOS concentration. In contrast, the melting latent heat decreased from 331 to 248.6 J/g due to the rise of TEOS concentration. After 100 thermal cycles, the melting latent heat of all samples was reduced, as exemplified by the 41.7 J/g latent heat reduction of samples with 3.9 g of TEOS. In addition, a sample with a 3.9 g of TEOS was cracked after 20 and 100 cycles, as depicted through SEM images.

Furthermore, Wei et al[83] focused on the development of void between Al_2O_3 shell and Al-Si/Bi core following the process described in Reference 15 by utilizing immiscible alloy Al/Bi as precursor material. Bismuth (Bi) basically acted as a catalyst, increasing the activity of the alloy particles and stimulating the production of a precursor shell on the Al/Bi surface. Bi also contributed significantly to the formation of void space through the evaporation of the majority of the outer Bi in Al/Bi alloys. According to the DSC curve, the prepared composite samples possessed multiple high melting points in the range 571.8°C to 631.9°C with the latent heat 209.5 to 278.2 J/g, which was lower than the sample without Bi. Additionally, the thermal conductivity of composite was in the range 2.068 to 2.734 W/m K, while 2.966 W/m K was obtained for the sample without Bi. After 300 thermal cycles, the latent heat of composite samples decreased by around 24.3 to 31.7 J/g, which was still less than the latent heat of the sample without Bi, which decreased by approximately 58.1 J/g.

Moreover, Wei et al[84] continued the microencapsulation of Al-Si alloy in Al_2O_3 shell based on the method in Reference 15. Varying quantities of TEOS (4.0, 4.5, and 5.0 g) were utilized during the calcination treatment in nitrogen (N_2), while 4.0 g of TEOS was used in argon calcination process. SEM images showed a rough and discontinuous surface for encapsulated PCM in argon, but a high dense and uniform surface for the sample containing 4.5 g TEOS N_2. Multiple melting temperatures were obtained for all samples in the range 571.5°C to 637.9°C with highest latent heat of 255.8 g/J was produced for the sample in argon. However, after 3000 thermal cycles, the latent heat was reduced by about 118.5 J/g for the sample in argon. Meanwhile, the latent heat for the sample in N_2 calcination were less reduced by about 59.8 to 77.7 J/g indicating denser and more uniform shell material due to the self-repair shell material.

Yolk/shell microsphere encapsulated Al in Al_2O_3 shell was prepared by Li et al[85] by the involvement of catalyst. Various amounts of nickel chloride (NiCl) were carried out to control the nickel species as catalyst on Al surface for improving the oxidation of Al by oxygen to form Al_2O_3. However, the relatively high concentration of NiCl potentially reduced the void space between Al and Al_2O_3 shell. Compared with the Al core material, the fusion enthalpy of MEPCM was lowered from 390.5 to 315 J/g with a good morphology structure at 663.5°C. The prepared sample obtained high thermal stability due to retained original shape after 50 cycles with a phase

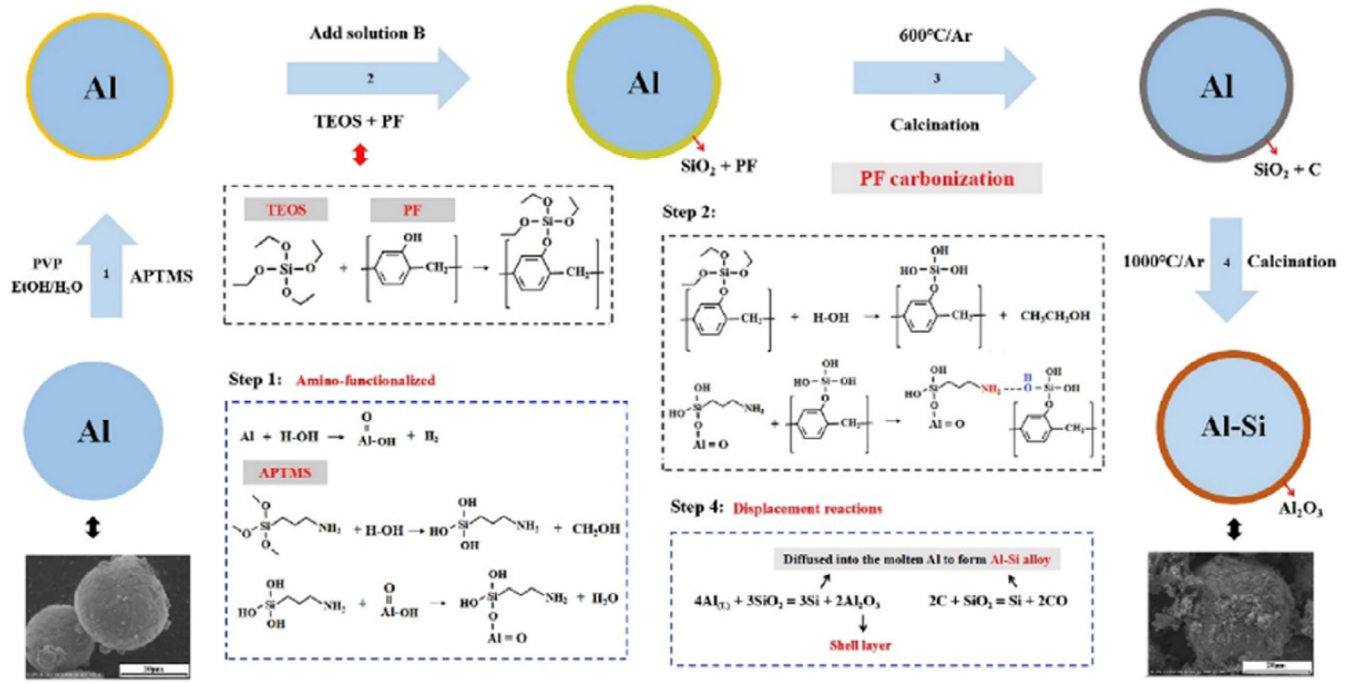

FIGURE 9 Schematic diagram of the preparation process of microencapsulated Al-Si with Al_2O_3 shell.[15] Reused with permission from Elsevier license number 5260850395043

transition temperature and latent heat of 663.6°C and 311.8 J/g, respectively. In addition, when the temperature was less than 600°C, the thermal conductivity remained constant at 1.5 W/m K, but rapidly increased as the temperature above the melting point of Al.

Bao et al[86] attempted to accommodate volume expansion of MEPCM by employing "double-layer coating, sacrificial inner layer" method. High-melting temperature tin with a melting point of 234.7°C was selected as PCM, and double layers of PMMA and SiO_2 were prepared as shell materials, as illustrated in Figure 10. Initially, tin was encapsulated by PMMA using ultrasonic, followed by sol-gel method to generate a second coating of SiO_2. The PMMA shell was subsequently degenerated at 400°C before finally sealing the pores of MEPCM. Compared with pure tin, the latent heat of MEPCMs with thermal expansion void was lowered from 60.22 J/g to 57.8 J/g at melting temperature of 235°C. Additionally, it was discovered that the latent heat values of MEPCMs with thermal expansion voids were almost identical to those of MEPCMs with the original core-shell structure up to 200 cycles. In comparison, the morphology of MEPCMs without a thermal expansion void amended drastically after 200 thermal cycles, with a 20% decrease in latent heat.

The "double-layer coating, sacrificial inner layer" encapsulation method was also adopted by Ma et al[87] using Sn microsphere PCM in a double-layer shell of PMMA and $CaCO_3$. After heating up to 400°C, the PMMA was decomposed to form the void between Sn and $CaCO_3$. When MEPCMs with or without voids were compared with Sn microspheres, there was no discernible change in the melting temperature at 231.8°C. However, the MEPCM without and with void lowered the latent heat of the Sn from 60.22 J/g to 58.06 J/g and 56.31 J/g, respectively. As a result of the encapsulation with a $CaCO_3$ shell, the supercooling of Sn was dramatically reduced by about 59.8% and 7.76% for MEPCM without and with void, respectively. Furthermore, SEM images were utilized to observe both MEPCMs after 200 thermal cycles, and it was determined that the MEPCM with void had a good shell structure and retained an unchanging latent heat of around 54 to 55 J/g. In contrast, the core-shell structure of MEPCM without void was entirely damaged, allowing the core material to flow out and resulted a 15.5% decrease in latent heat. The MEPCM with void was subsequently combined with ceramic material of glass frit (GF) and Al_2O_3 sintering agent to achieve higher thermal storage from sensible heat, and it was observed that the composite MEPCMs was maintained in spherical structure and uniform distribution. As the introduction of ceramic, the latent of MEPCM was reduced by approximately 50.7% with high thermal conductivity at 3.60 W/m K.

A "solvent evaporation-heating curing" method was introduced by Wang et al[88] to encapsulate Al-Si PCM in SiCN shell material. Basically, solvent evaporation was carried out intially by mixing Al-Si, precursor shell

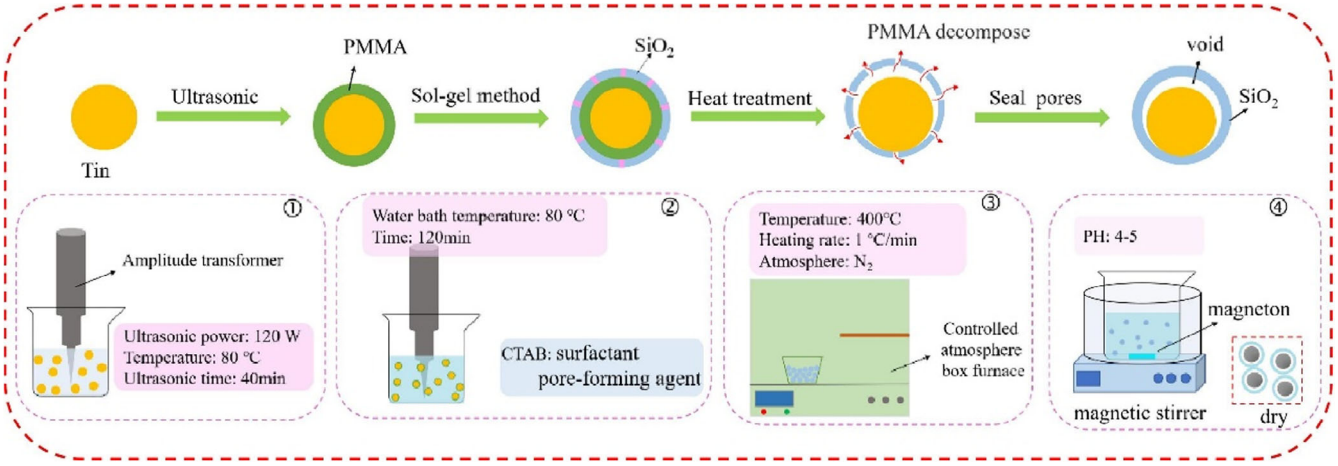

FIGURE 10 Fabrication process of MEPCM with "double-layer coating, sacrificial inner layer" technique.[86] Reused with permission from Elsevier license number 5260850532724

material of organic polysilazane (OPSZ) followed by heating curing of solution up to 700°C at argon atmosphere to generate SiCN shell material. Varying core-shell mass ratios were prepared and it was obtained that the core-shell mass ratio of 4:1 achieved regular spherical shape without agglomeration. The MEPCM had a melting point and latent heat of 573.7°C and 281.2 J/g, respectively, which was slightly lower than PCM's melting temperature of 575.8°C and latent heat of 318.6 J/g. Based on DSC result, it was also shown that the SiCN could reduce the supercooling effect of Al-Si from 6.8°C to 1.8°C. They also reported that the heat charging/releasing rate of Al-Si was reduced as the quantity of shell materials rose from 84.96 J/g min to 47.94 until 72.35 J/g min. Interestingly, after 100 thermal cycles, the melting and freezing enthalpy of MEPCM dropped only by approximately 3.8% and 6.2%. Interestingly, after 100 heat cycles, the melting and freezing enthalpies of MEPCM dropped by approximately 3.8% and 6.2%, correspondingly.

3.7 | Comparison of microencapsulation techniques

Shell material selection is crucial for encapsulating medium and high-melting temperature PCM. Liquid metal and molten salt PCM generally exhibit high chemical corrosion in the presence of shell materials like metals.[13] The transition of high-melting temperature PCMs from solid to liquid leads to the volume expansion of capsule, which results in thermal stress.[89] However, fabricating MEPCMs with thick shells will decrease the heat storage density. Therefore, the shell material for most of the low-temperature MEPCM might not be capable of withstanding medium and high temperatures due to the difficulties aforementioned. Thus, inorganic shells, as shown in many studies, are required with temperature degradation above the medium and high-melting temperature of the PCM. Other studies considered the use of polymer shell materials; however, they have relatively low thermal stability and thermal conductivity. Numerous approaches also have been devised to create space between the core and shell materials in order to appease volume expansion during phase transition.

Many studies have introduced various methods to encapsulate medium and high-melting PCMs. Each method has its own characteristics and can be utilized based on needs. Chemical method using polymer shell material is extensively used to encapsulate various types of PCMs. The widely used polymer shell materials include polymethyl methacrylate (PMMA), polystyrene-butyl acrylate (PSBA), polyethyl-2-cyanoacrylate (PECA), and polyurethane. However, the encapsulation of salt hydrate PCMs using chemical method is more complicated as compared with paraffin PCMs due to their hydrophilicity and water content nature. In the sol-gel technique, tetraethylorthosilicate (TEOS) is widely used as a precursor via hydrolysis and condensation to create silica shell. Hydrothermal followed by heat-oxidation method could also be employed for encapsulating medium-high melting temperature PCMs, such as Al-Si and Zn-Si alloy in α-Al_2O_3 or θ-Al_2O_3 shells. Unfortunately, the fabrication process of a boehmite treatment and heat-oxidation treatment is only applicable to Al-Si and Al-Zn alloy microcapsules. Finally, the benefits and detriments of each method are summarized in Table 9.

TABLE 9 The comparison of microencapsulation techniques of PCM with medium- and high-melting temperature

	PCM			MEPCM						
	Type	T_m (°C)	Δh_m (J/g)	Shell material	T_m (°C)	Δh_m (J/g)	Particle size (μm)	Encapsulation efficiency (%)	Advantages	Disadvantages	Reference
Emulsion/ miniemulsion	Stearic acid	66 to 83	189	PMMA, PMMA-MA, PMMA-HEA, PMMA-SiO_2, PMMA-S	60 to 89	50 to 189	110 to 360 nm	26.5 to 38.9	Bio-based fatty acid PCM	Low encapsulation efficiency	40
	RT 80	85.1	161.1	Polystyrene-butyl acrylate (PSBA)	78.4 to 84.1	4.9 to 23.9	52 to 112 nm	78 to 80	High thermal stability	—	14
	$Mg(NO_3)_2{\cdot}6H_2O$	89	162.8	Poly(ethyl-2-cyanoacrylate) (PECA)	91	83.2	100 to 200 nm	52	• Supercooling reduction • Structural integrity improvement • Prevention of incongruent melting	Corrosivity	63
	$Mg(NO_3)_2{\cdot}6H_2O$ and $Na_2SO_4{\cdot}10H_2O$	89 and 32	162.8 and 228.1	PECA	32 to 94	29.1 to 138.6	100 to 200 nm	—	• Supercooling reduction • Multiple melting and freezing temperature	Corrosivity and relatively low thermal conductivity	64
	$Mg(NO_3)_2{\cdot}6H_2O$	89	162.8	SiO_2 via Pickering Shell	~90	112.8	500 to 750 nm	—	High thermal conductivity compared with polymer shell material	Supercooling	90
pcInterfacial polymerization	Erythritol	121	—	Polyurethane	121	82	10 to 200	82	Supercooling reduction due to the agent addition	No thermal cycle testing	65
Sol-gel	$NaNO_3$	306.8	158.1	SiO_2	294.2 to 293.4	25.1 to 29	0.2 to 1	11.4 to 15.7	No significant change of latent heat	Easily influenced by morphology and core/shell ratio that lead to the effectiveness of MEPCM	67
	Na_2SO_4	886.24	182.3	SiO_2	886.84 to 890.48	104.6 to 211	400	—	Good long-term thermal stability	Evaporation mass loss	12
	KNO_3	334	100.3	SiO_2	334	95.48	~10	94.1	• High thermal reliability and stability • High encapsulation ratio	—	66

TABLE 9 (Continued)

	PCM			MEPCM							
	Type	**T_m (°C)**	**Δh_m (J/g)**	**Shell material**	**T_m (°C)**	**Δh_m (J/g)**	**Particle size (μm)**	**Encapsulation efficiency (%)**	**Advantages**	**Disadvantages**	**Reference**
	Indium	156	28.5	SiO_2	155.3	19.6	90 to 165 nm	—	Enhanced thermal performance	—	91
	Li_2CO_3-Na_2CO_3	498.6	360.5	SiO_2	498.6	250.9	5.1 ± 2.1	69.6	• Tunable melting point and latent heat • Effective heat capacity enhancement	• Incongruent melting behaviour High cost	68
	Al 87.48 to 12.06 wt% Si	—	504.95	Al_2O_3	~558	307.21	100	103 to 108	—	Low durability	69
Spray drying	KNO_3	338.5	82.09	ZnO	328.5 to 336.1	35.78 to 63.36	20 to 50	51 to 78.2	Corrosion reduction	No thermal stability testing	53
	KNO_3	338.1	140.4	ZnO	328.3 to 339.1	47.2 to 100.9	1 to 2	32.7 to 63.6	Long-term durability	—	71
Fluidized bed	Bischofit	108.5	104.5	Acrylic	104.6	95	—	87.02	High encapsulation efficiency	No thermal stability testing	73
	$MgCl_2 \cdot 6H_2O$	117.1	127.2		95.3	118.3	—	92.22			
Hydrothermal method followed by heat oxidation	Al-25 wt% Si	577	432	α-Al_2O_3	573	247	40.7	—	• High heat storage density • Resistant to corrosion	Low-strength shell	74
	Al-25 wt% Si	577	432	α-Al_2O_3	579	233	36.4 to 37	—	High cyclic durability	—	75
	Al	660	384	α-Al_2O_3	660	273 to 301	36.1	—	Higher cyclic durability compared with Reference 74	Need improvement for practical use	76
	Al-25 wt% Si	577	432	α-Al_2O_3 and θ-Al_2O_3	—	183	—	—	High durability and thermal stability	Limited on particular PCM	77
	Al	660	384	α- Al_2O_3	660	166-186	42.6	43.2 to 71.1	• Durability about 300 cycles • Self-repaired shell • Void creation	Exploration in coating thickness	78
	Al-25 wt% Si	574	343	Al_2O_3 and Cu	570	100	36	—	Low breakage ratio	High reduction latent heat after 100 cycles	79
	Al	660	384	Al_2O_3 and Cu	659.6	223.4	—	—	Smooth and dense shell	Relateviley low thermal cycles	80
	Al-10 wt% Zn	643	176	Al_2O_3, ZnO and Cu	638.6	89	15 to 40	—	Durability about 50 cycles	Latent heat reduction after 50 cycles	10

(Continues)

TABLE 9 (Continued)

	PCM			MEPCM							
	Type	T_m (°C)	Δh_m (J/g)	Shell material	T_m (°C)	Δh_m (J/g)	Particle size (μm)	Encapsulation efficiency (%)	Advantages	Disadvantages	Reference
	Zn-30 wt% Al	440 to 512	166	Al_2O_3	437–512	117	—	—	—	Heat capacity decrease	81
Solvent extraction and ultrasonic dispersing	$NaNO_3$	306.43	188.2	Perhydropolysilazane (PHPS)	306.19 ± 0.1	159.2 ± 2.4	95.6	83.8	High encapsulation ratio	Few works to encapsulate PCM	82
Mixing and sintering	NaCl/KCl	665	259.6	Diatomite	661	179.3	—	—	High thermal stability	Tendency of enthalpy loss as the increase thermal cycle	13
Synthetic methodology	Al-Si	—	—	Al_2O_3	573.9 to 641.4	248.6 to 331.0	35.7 to 130.8	—	Tunable melting temperature	—	15
	Al-Si/Bi	—	—	Al_2O_3	571.8 to 631.9	209.5 to 278.2	39.3 to 131.3	—	High thermal conductivity	Reduced latent heat after 300 thermal cycles	83
	Al-Si	—	—	Al_2O_3	570.6 to 637.9	165.4 to 255.8	37.2 to 78.5	—	• Self-repair shell material • Multiple melting temperatures • High durability	—	84
Yolk/shell	Al	660	390	Al_2O_3	663.5	315	27.3	—	• High thermal conductivity • High thermal stability • Void creation	Complex chemical processes to construct (Fe_2O_3/Al_2O_3)/(Al@ Al_2O_3	85
Double-layer coating, sacrificial inner layer	Tin	234.7	60.22	SiO_2	235	57.8	—	—	• Void creation • High thermal stability up to 200 cycles	Complex processes	86
	Sn microsphere	231.8	60.22	$CaCO_3$	231.8	56.31	30 ± 15	93.5	• Void creation • Supercooling reduction • High adaptability for different applications	Supercooling	87
Solvent evaporation-heating curing	Al-Si	575.8	318.6	SiCN	573.7	281.2	16.9 to 93.8	87	• Relatively simple encapsulation technique • Supercooling reduction	Supercooling	88

4 | THERMAL ENHANCEMENT PCMS

The potential of medium-high melting temperature PCMs is often limited by barriers such as low thermal conductivity and low efficiency of PCM storage systems. Some past studies have therefore looked at various methods of enhancing their thermal conductivity with materials such as metal particles, carbon, and ceramic-based additives. Regarding low efficiency, the concept of multiple storage arrangement systems has been investigated as means of improving the overall efficiency of medium-high melting PCM storage systems.

4.1 | Thermal enhancement

4.1.1 | Metal-based additives

This was exemplified in the work undertaken by Zhang et al.[92] They investigated experimentally and numerically the heat transfer of composite eutectic salt PCM (50 wt% $NaNO_3$, 50 wt% KNO_3) by introducing copper and nickel metal foams for the enhancement of thermal conductivity. To minimize thermal contact resistance with the metal foam, the metal foams were manufactured into a cylindrical shape in milli scale that was slightly bigger than the inner diameter of the PCMs. The composite eutectic PCM system was subsequently heated from 30°C to a particular temperature, and vice versa for cooling process, to observe the thermal improvement. The results in Figure 11A,B show that there was about 19.3% and 28.8% reduction in the time-durations of heat transfer during heating and cooling processes, respectively, for the composite PCMs compared with the pure eutectic PCMs in temperature difference of 210°C.

Li and Wu[93] studied numerically the thermal performance of $NaNO_3$ with high thermal conductivity copper by optimizing the porosity and pore density matrix. The PCMs were inserted into the porous metal matrix with cube-shaped matrix structures. Under steady and unsteady heat transfer conditions, eight distinct porous copper matrices were examined, each with two porosities (90% and 95%) and four pore densities (5, 10, 20, and 30 pores per inch [PPI]). The effects of heat conduction and natural convection on the heat transfer inside the PCMs system were investigated under steady-state conditions. The results indicated that heat conduction transfer was magnified by around 28.1 times in the solid state, but improved by 3.1 times in the liquid phase due to the presence of natural convection and heat conduction. These magnifications associated with the shorter duration during melting and solidification of composite PCMs, which was studied under unsteady state. It was reported that they were able to achieve a 20% reduction in the minimum melting time for $NaNO_3$ implanted with 90% porosity and 10PPI compared with pure $NaNO_3$. Meanwhile, the shortest solidification time for $NaNO_3$ implanted with 90% porosity and 30PPI was only 3.9% of the time required for pure $NaNO_3$ throughout the solidification process.

Yang et al[94] studied numerically the thermal behaviour of $NaNO_3$ PCMs with copper metal foam. The porous copper foam, which was filled by Na_2SO_4, was contained by a rectangular domain with a length (y) of

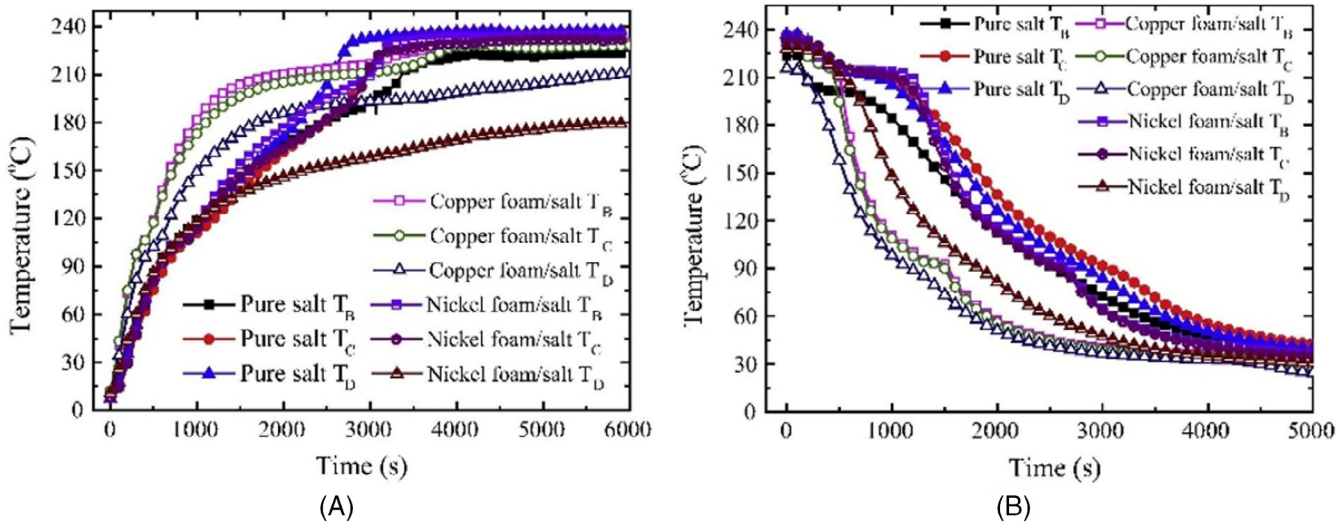

FIGURE 11 Temperature profile during (A) heating and (B) cooling process.[92] Reused with permission from Elsevier license number 5260850678157

30 cm and a width (x) of 10 cm. Various copper foam samples with varied geometric features, such as porosity (ε), average porosity ($\bar{\varepsilon}$), and pore density (ω), were examined and studied. Simulation result showed the 13.8% shorter melting time of samples with ε increasing from bottom to top compared with constant ε at 0.9, and it was 24.2% shorter than that of samples with ε decreasing from bottom to top. The temperature variation of chosen places in materials with increasing porosity from bottom to top was also able to uniformize the thermal field, according to the findings.

Yuan et al[95] investigated the improvement of aluminate cement as a TES material with a melting point of 282.2°C utilizing Cu particles in concentrations ranging from 1 to 15% wt. After dispersing the copper particles and polycarboxylate in water, the mixture was introduced to the PCM for the hydration process. It was observed that the thermal conductivity improved by the addition of Cu particles and reduced as the temperature rose. The best thermal conductivity values after heat treatment were achieved at Cu powder concentration of 15 wt%, which exhibited 24%, 50%, and 51% greater than that of pure PCM at 105°C, 350°C, and 900°C, respectively. According to the DSC curves, there were two major endothermic peaks at 282.2 and 696.8°C, respectively, caused by the dehydration product of TES. Similarly, endothermic peaks associated with TES dehydration emerged at about 280°C in the composite PCM containing Cu particles. Dehydration of the products was also found to result in a 13.7% mass loss in pure PCM. Meanwhile, the continuous oxidation process in composite PCM resulted in a weight rise of 1.5%.

The improvement of convective heat transfer of MEPCM was numerically investigated by Benner et al.[96] Tin, aluminium, and copper were separately analysed as core materials in the fused silica shell material. Encapsulation of PCM was characterized by different ratio of shell thickness and core (ϕ). It was concluded that the convective heat transfer rate was improved as the rise of ϕ as a result of the increase in surface area. However, when ϕ rose, the ratio of latent heat (LHR) to total energy storage declined, indicating that sensible heat was the predominant energy held inside the particle due to convective heat transmission. Among those PCMs, copper's LHR was the lowest. In addition, the time required to commence the melting process ($t_{\text{heat up}}$) was utilized to define the transient process, followed by the time required to complete the melting process (t_{melting}). The $t_{\text{heat up}}$ for tin and aluminium grew as ϕ increased, but the $t_{\text{heat up}}$ of copper was firstly reduced before progressively increasing. This difference was attributed by the fact that the thermal time constant changed as a function of convective thermal resistance and lumped thermal capacitance. Additionally, the t_{melting} dropped as ϕ raised for all cases, which corresponded to the rapid cooling rate associated with the thicker shells' higher surface area.

4.1.2 | Carbon-based additives

Another material that may be utilized to improve the thermal performance of PCMs is carbon-based. Aside from excellent thermal conductivity, carbon materials have the potential to be employed owing to their non-corrosive properties, light weight, and reduced density, which metal-based materials do not have. Carbon substances are also employed because they have desirable properties, such as high stability and PCM compatibility.[97] Carbon fibre, carbon nanotubes, graphite, and graphene are all extensively utilized to enhance the thermal conductivity of PCM.

Expanded graphite (EG) was adopted by Tian et al[58] to intensify the heat transfer performance of binary eutectic chloride (NaCl-$CaCl_2$) by impregnation of molten eutectic PCMs in porous EG at high temperature. They investigated and evaluated various concentrations of EG ranging from 0.5 to 20 wt% and determined that the maximum EG content in the compound should be 7 wt% to avoid any leakage. When the EG concentration was less than 3 wt%, the specific heat capacity of composite PCMs declined with increasing EG content in the liquid state. Once the EG concentration exceeded 3 wt%, it began to rise rapidly. Although the phase change temperatures of composite PCMs varied little in the range of 775-780°C, the phase change latent heats decreased linearly with the EG content by about 3 until 19.24%. The thermal conductivity of composite PCMs containing 0.5 to 20 wt% EG was increased by 123.2% to 701.1% as compared with binary eutectic PCM. Another important discovery was that composite PCMs had a greater heating and cooling rate than binary eutectic chloride due to the enhanced heat transfer rate caused by the EG component. The composite PCMs/EG could reduce the melting and solidification time by about 11.54% to 23.85% and 23.63% to 32.72%, respectively, than that of pure eutectic PCM. They determined that, when all heat storage properties were considered, the EG content of composite PCMs should be between 7 and 10 wt%.

Shape stable PCMs (SSPCMs) were adopted by Wang et al[98] using high-melting temperature Na_2CO_3-K_2CO_3 as PCM, while coal fly ash and EG served respectively as ceramic skeleton material (CSM) and thermal conductivity enhancer. The mixture was fabricated under high pressure and temperature by maintaining the PCM to CSM at 7:3, while EG was prepared in the range of 1.5 until 6 wt%. It was observed that the more EG content in

the composite, the lower the latent heat. Due to the introduction of EG, the latent heat of composite was reduced by about 32.98% until 36.77% at a nearly constant melting temperature about 700°C. On the other hand, when the EG content was 6 wt%, the thermal conductivity of the composite was enhanced to a maximum of 183% with a 5% drop in heat storage density compared with SSPCM without EG.

Ran et al[99] prepared and characterized a high-temperature composite of eutectic salt-based PCM in a supporting matrix material of α-Alumina and EG additives. A mixture of NaCl, KCl, and $MgCl_2$ was selected as the PCM with a melting point of 471.8°C and 251.06 J/g of latent heat. The composite was prepared with a uniaxial compression method with varying amount of graphene from 5 to 15% wt. It was demonstrated that the EG effectively enhanced the composite's thermal conductivity by means of 2.47 to 6 times. Due to the addition of 15% wt EG, the latent heat of composite was 91.32 J/ g at a melting temperature of 471.8°C. After 300 thermal cycles, the latent heat reduced to 86.98 J/g, while the melting temperature remained almost constant.

Shape stabilized composite phase change material (SS-CPCM) was prepared by Soleimanpour et al.[100] Sodium nitrate ($NaNO_3$) with melting point 308°C was selected as PCM, while supporting material was developed by employing diatomite. The thermal performance of SS-CPCM was improved by the introduction of nano EG and subsequently compared with nano diamond additives. The SS-CPCM was produced by uniformly mixing the $NaNO_3$, diatomite, and additive prior to moulding them at different pressures. Various composition of SS-CPCMs were prepared and optimized according to the phase change temperature and phase change time stability as design of experiment. It was found out that the optimized SS-CPCM was achieved with the composition of $NaNO_3$ and additives as 62.9% and 3.99%, respectively, at pressure of 330 bar. The melting point of composites was obtained at 302.03°C and 302.14°C for $NaNO_3$/diatomite/Nano EG SS-CPCM and $NaNO_3$/diatomite/nano diamond, respectively, with corresponding enthalpy of about 87.32 and 90.51 J/g. IR-camera was utilized to investigate the thermal performance and obtained 60 seconds as the most stable time in phase transition. In addition, nano diamond showed a slightly better thermal performance compared with the nano EG.

Kim et al[101] analysed the heat transfer of $MgCl_2$ as PCM with melting temperature of 714°C by employing graphite foam to enhance the thermal performance of PCM. A system with capacity of 75-MW concentrated solar power (CSP) facility was constructed using a storage tank, a PCM/graphite foam composite, and vertically oriented pipes conveying a heat transfer fluid (HTF) to discharge the heat during solidification. For a PCM/graphite foam system, the addition of the graphite foam established a 30 W/m K effective thermal conductivity, allowing the number of pipes to be reduced from 11 427 to 839 resulting in significant cost savings.

Hybrid vacuum and pressure-assisted infiltration were demonstrated by Lan et al[102] to infuse high melting PCM into graphite foams. Molten chloride salt blend with melting temperature of 355°C and 200 kJ/kg of energy storage density was selected as the PCM. Intially, the PCM infiltration was regulated under vacuum condition. Pressurization with nitrogen up to 1100 kPa was subsequently carried out at temperature of 500°C. The efficiency of infiltration was obtained more than 90% with thermal conductivity improvement, about 45 times that of pure PCM. However, it was found that the percentage of energy density loss was approximately 30.05%. The comparison weight of infiltrated samples before and after cycling was evaluated to determine the thermal stability, and it was found 18% loss of sample after multiple cycles.

Singh et al[103] developed a composite of $MgCl_2$ and graphite foam using infiltration process. High density (HD) and low density (LD) graphite foams were adopted for thermal conductivity enhancement of PCMs. Thermal conductivity was calculated by relating to measured thermal diffusivity, density, and specific heat capacity at constant pressure. They reported that the composite $MgCl_2$/HD and $MgCl_2$/LD resulted in thermal conductivity enhancement by about 200 and 30 times that of pure $MgCl_2$, respectively. Based on DSC test, due to the presence of HD and LD foam, the melting point of pure $MgCl_2$ was slightly lowered from 714°C to 709°C. However, the heat fusion of pure $MgCl_2$ was significantly reduced by about 50.17% and 21.77% from 353.6 to 225.2 J/g and 353.6 J/g for $MgCl_2$/HD and $MgCl_2$/LD foam, respectively. Additionally, it was demonstrated a small reduction in the $MgCl_2$/HD and $MgCl_2$/LD mass ratios after 100 cycles of approximately 4.1% and 2.7%, respectively, confirming the correctness of the infiltration rate calculation.

Carbon fibre was selected by Zou et al[104] to support Al matrix composite with a self-encapsulated silicon structure through rotating magnetic field. Various weight percentages of Si were utilized to prepare Al-Si alloy, and it was obtained the thermal conductivity improvement of shell from 65.2 to 100.7 W/m K as the increase of the Si content in initial Al-Si from 25 to 40 wt% of Si. They determined that 30 wt% of Si was the optimum composition due to comprehensive properties of heat absorption capacity and ultimate damage temperature. Additionally, it was observed that the latent heat and melting point of

the composite were between 455.4 and 480.9 J/g and 586°C and 594.2°C, respectively, at various heating rates.

An experiment using graphite powder was adopted as reinforced and thermal enhancer material by Zhong et al[105] to encapsulate NaCl PCM utilizing quasi-isostatic pressing technique. The high-melting temperature NaCl was combined with 40 wt% graphite powder and 10 wt% cellulose particles. After heat treatment at 850°C, the cellulose was burned away to create void and provide thermal expansion during phase transition of PCM. The latent heat of the composite was lowered from 294 to 159.6 J/g when compared with NaCl, but the melting point remained nearly constant at 803°C. Meanwhile, the thermal conductivity of composite was 13.93 W/m K, approximately 34 times that of NaCl. Moreover, numerical study was carried out to observe the heat performance of composite during charging and discharging process. It was discovered that after 99% of the storage capacity of each system was attained, the thermal performance of the composite NaCl and graphite was respectively 92.5% and 168.4% greater than that of pure NaCl during charging and discharging process.

Expanded natural graphite treated with sulphuric acid (ENG-TSA) was employed by Zhao et al[106] to improve the thermal conductivity of eutectic PCM, $KNO_3/NaNO_3$, by cold-compression method. The eutectic PCM was initially dissolved in water, and the solution was gradually absorbed by the ENG-TSA particles via mechanical stirring. After drying in the oven, the composite materials were pressed using a mechanical equipment. The effective thermal conductivity of nitrates/ENG-TSA composites was found to be considerably greater than that of nitrates/ENG composites in Reference 107, with the greatest magnification around 110 times that of pure nitrates. The addition of ENG-TSA to the PCM resulted in a slight decrease in latent heat of around 10.1% and 15.4%, respectively, but no significant variation in phase change temperature, according to the DSC thermogram. However, the segregation remained a major issue in this study, resulting in excessive pore pressurization.

Zhao and Wu[108] studied the thermal transport enhancement of $NaNO_3$ as PCMs using metal foam and EG during charging and discharging processes. Copper and copper-steel alloy with different porosity were utilized for metal foam, while 3 wt% of EG was mixed and stirred with the molten PCMs. During the first heating phase, the temperatures at specific points (T_3) in containers filled with PCMs containing metal foams and EG were greater than that within container with pure PCMs. Metal foams and EG structures, on the other hand, decreased the total heat transfer rate once PCMs were entirely melted owing to the restrained natural convection effect. Similar with charging process, metal foams and EG improved the discharging process of PCMs with maximum time reduction of about 63.12% than that of pure $NaNO_3$. Additionally, decreased porosity metal foam was able to mitigate the detrimental effect of natural convection by increasing heat conduction, which therefore enhanced composite heat transfer. As a result, they determined that metal foams with 90% porosity and 20 ppi outperformed EG in terms of overall performance.

Furthermore, Wu and Zhao[109] continued the investigation of thermal performance enhancement for $NaNO_3$ using metal foam (MF), EG, and their mixture. They modified the heating condition by installing the heater on top of container, a technique known as top heating, and compared it with the bottom heating as described in Reference 108. In the melting process, similar to the result in Reference 108, the heat transfer rate of metal foam with a porosity of 90% and a PPI of 20 (MF2) was greater than that of other composites and pure $NaNO_3$. Top heating was subsequently carried out and ΔT_{max} was defined as the maximum temperature difference inside the liquid $NaNO_3$ to examine the total heat transfer performance and the role of the natural convection. It was demonstrated that the heat transmission rate of the metal foam composite under the top heating conditions was 120% higher than that of pure $NaNO_3$.

4.1.3 | Ceramic-based additives

Ceramic-based materials have also been investigated for the thermal enhancement of medium and high-melting temperature PCMs.

Gokon et al[110] investigated the use of MgO-ceramics with molten alkali-carbonate of Na_2CO_3, K_2CO_3, and Li_2CO_3 in a double-wall solar reformer tube. To postpone the temperature decrease of a catalyst bed, the annular area between the outer tube wall and the interior catalyst tube of a double-walled reactor was filled with the composite material of MgO and molten PCMs. The heat-discharge of Na_2CO_3 was used to avoid a quick temperature fall of the interior tube while using the 100 wt% Na_2CO_3 molten salt. Additionally, the temperature of the interior tube was greater for the composite than for pure Na_2CO_3, despite the fact that the less Na_2CO_3 in 80 wt% Na_2CO_3/MgO composite material than the pure Na_2CO_3 molten salt. Moreover, after 30 minutes of cooling, the alumina-bed temperature was about 700°C without the composite material, but it was 760°C, 750°C, and 730°C with the composite material for Na_2CO_3/MgO, K_2CO /MgO, and Li_2CO_3/MgO composite, respectively. According to this finding, they conclude that a composite with a higher melting point was potentially used as a thermal storage medium in a double-walled reactor.

Ge et al[111] developed a composite material made of a eutectic salt of sodium carbonate and lithium carbonate, along with MgO ceramic and graphite for support and thermal enhancement, respectively. These materials were combined and then cold compressed into slabs before being sintered in an electric furnace with a mass ratio of 0.25:1:1 for the graphite, the carbonate salt, and MgO, respectively. The composite melted in the temperature range of 496 to 507.1°C, which was not appreciably different from pure eutectic PCMs. Meanwhile, the composite had a latent heat of around 178.3 J/g, which was almost half that of the pure salt. A self-built automated apparatus was used to test the cycle heating-cooling performance of the composite materials, and the result during charging and discharging was recorded. It was demonstrated that the composite had a greater thermal conductivity than pure eutectic PCMs due to the composite reaching 600°C in approximately 442 seconds less time than pure eutectic PCMs during the melting process. After cooling from 680°C to 390°C, the discharge period of composite was similarly shorter than that of pure eutectic.

The SiC ceramic honeycomb (SCH) with high thermal conductivity was utilized by Li et al[112] to advance the heat performance of alkali nitrate mixture by employing vacuum infiltration. In this study, the mixture of $KNO_3/NaNO_3$ was selected as PCM with the melting temperature and latent heat of 226°C and 106.3 J/g, respectively. The composite included 0 to 30 wt% SCH, and it was discovered that the composite containing 30% SCH had a melting point that was indistinguishable from that of pure nitrate mixture. Meanwhile, composite PCMs exhibited a somewhat lower latent heat value of 72.8 J/g than pure PCMs. The thermal performance of the composite revealed that increasing the mass percentage of SCH in the PCMs resulted in a faster melting and solidification process, as seen in Figure 12. When 30, 23, or 18 wt% of SCH was added to the composite PCMs, the heat storage duration was reduced by 52.8%, 38.0%, and 32.8%, respectively, while the heat release time was lowered by 58.3%, 48.6%, and 47.2% compared with the pure PCM.

Wang et al[113] selected SiN_4 ceramic skeleton material to construct shape stabilized eutectic salt-based PCM by pressure impregnation. The salt of ternary chloride (ClNaKMg) was prepared to have a composition of 50 wt % NaCl, 30 wt% KCl, and 20 wt% $MgCl_2$, with a melting temperature and latent heat of 471.2°C and 258.7 J/g, respectively. Due to the introduction of SiN_4, the latent heat of composite was lowered by approximately 63.85% while maintaining a nearly identical melting point to the eutectic PCM. The thermal stability of composite was determined according to thermal properties after 300 thermal cycles, and the composite's latent heat declined by 9.3% at a melting point of 471°C. Additionally, they discovered that the addition of porous SiN_4 effectively increased the thermal conductivity of the composite by more than six times that of eutectic salt PCM.

Boron nitride (BN) additive was selected by Zhang et al[114] to improve the thermal energy storage and thermal performance of eutectic sodium nitrate ($NaNO_3$) and potassium nitrate (KNO_3). The eutectic PCM had multiple melting temperatures of 114.09°C and 221.54°C as the phase transition of soli-solid and solid-liquid, respectively. Various compositions of BN and eutectic PCMs were prepared through high-temperature static melting method. The composite PCM with 0.8 wt% of BN was

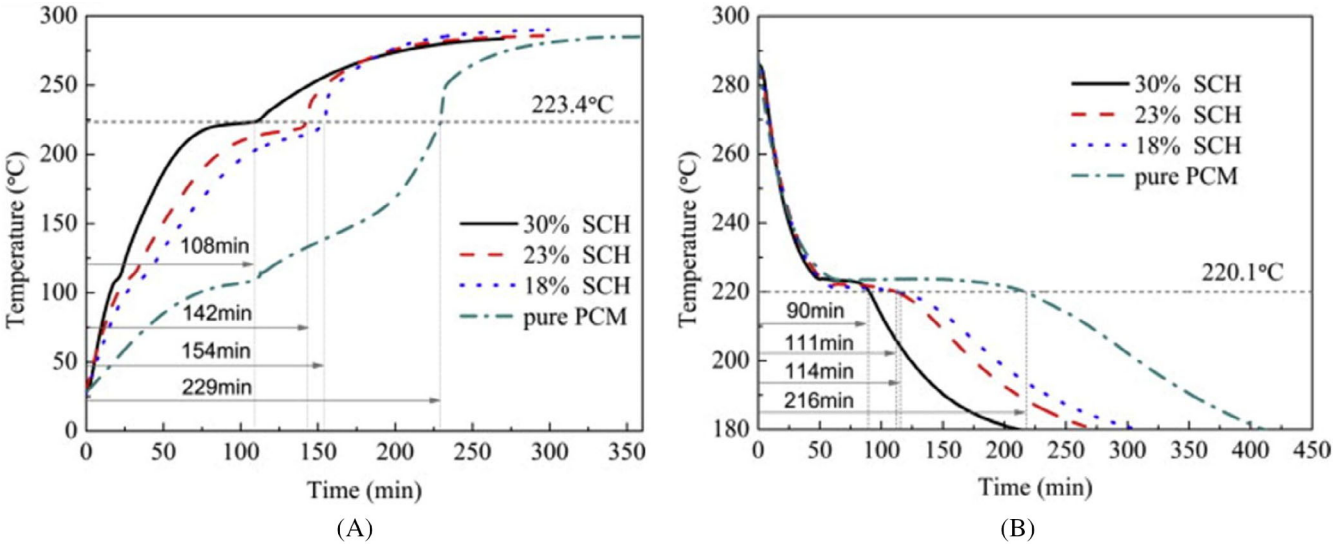

FIGURE 12 Temperature profile during (A) charging and (B) discharging process.[112] Reused with permission from Elsevier license number 5260850932736

reported as the optimum mixture due to the 16.03% of specific heat enhancement compared with the sample without additive. The 0.8 wt% of BN additive in PCM was also capable of improving the thermal conductivity of eutectic PCM from 0.27 to 0.32 W/m K with a high thermal stability.

4.2 | Energy storage efficiency enhancement

Multiple PCM arrangement is one of the methods that could be employed to enhance the thermal performance of PCM energy storage systems. For instance, Peiró et al[115] evaluated experimentally the advantages of multiple PCM configuration. Hydroquinone (HYD) and d-mannitol (DMA) were selected as PCMs with melting temperature in a temperature range of 150°C to 200°C. The storage tanks were constructed utilizing the shell-and-tubes heat exchanger principle, with PCM contained within the shell's casing and heat transfer fluid (HTF) circulating within the bundle of tubes. Three configurations were investigated: (a) a single PCM of HYD, (b) a single PCM of DMA, and (c) multiple PCMs of HYD and DMA. The effectiveness parameter of heat performance was defined as the ratio of real heat released over the theoretical maximum heat that may be discharged from PCM, using the inlet/outlet HTF temperature and the melting point of PCM. The inlet and outlet temperature of HTF were measured and it was recorded that the greater the difference in temperature between the input and output HTF temperatures, the faster the heat transfer. According to the HTF profile, a factor of four increase in the average heat transfer rate could be attained by applying the multiple PCM storage arrangement. Additionally, an average increase of 19.36% in efficacy over the single PCM setup was potentially attained by the twin configuration.

Elsanusi and Nsofor[116] investigated numerically the thermal performance of multiple PCMs at different configurations and compared subsequently with single PCM. Three different PCMs with melting temperature in the range of 170°C to 244.12°C were arranged in series and parallel. With conduction and natural convection included, it was observed that both series and parallel configurations improved performance marginally when compared with a single PCM structure, with a melting time decrease of around 15.5% and 9.3%, respectively. Additionally, the use of several PCMs reduced not only the overall melting time, but also increased the total energy stored, which was about 25% larger than the stored energy in the single PCM configuration.

Wang et al[117] studied the zigzag configuration of serial multi-PCMs (m-PCMs) to provide more interaction between high-melting point PCM, heat exchanger, and heat transfer fluid. A two-dimensional mathematical model was constructed for the charging process, and six sets of m-PCMs with varying melting temperatures were chosen for the modelling research, with the difference in melting temperatures between PCM-1 and PCM-3 (ΔT) ranging from 20 to 100 K. The results were compared with those obtained at $\Delta T = 0\,K$ (a single PCM only). The effectiveness (η) of m-PCMs was subsequently formulated as the ratio of the total heat stored in m-PCMs to that in a single PCM. These findings revealed that η was greater than one for the majority of the charging process, resulting in an overall process intensification via the usage of m-PCMs.

Michels and Pitz-Paal[118] studied numerically the heat transfer behaviour of cascaded latent heat storage (CLHS) for parabolic through solar power plants by employing five PCM segments compared with single PCM during charging and discharging process. The CLHS was set up based on Figure 13 and compared with single latent heat storage (LHS) of "All $NaNO_3$", "All KNO_3," and "All $MgCl_2$/KCl/NaCl." The storage outlet temperature was restricted while charging by the maximum operating temperature of the heat transfer oil, which could be surpassed when heated in the parabolic trough loop. Meanwhile, the temperature of the storage outlet during discharge was restricted by the linked Rankine cycles. In comparison to all other configurations, "All $NaNO_3$" demonstrated the largest storage capacity, about 74 MJ, with a very little part of PCM mass subjected to a phase shift at 8%, but the outlet temperature

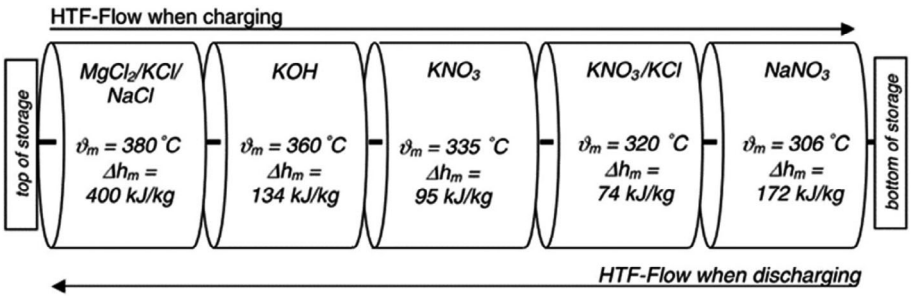

FIGURE 13 Scheme of CLHS test.[118] Reused with permission from Elsevier license number 5260860007218

surpassed the maximum allowed level at the end of discharging. Meanwhile, the CLHS had the largest phase change fraction, about 47% with an acceptable storage capacity, approximately 64.5 MJ. Another interesting finding was that the consistency of the HTF exit temperature of CLHS during charging and discharging was noticed when compared with the other configurations without exceeding the permissible maximum and minimum temperature.

Zhao et al[119] analysed numerically the thermal performance of TES system for applications to concentrated solar power (CSP) plants. The exergy efficiency was carried out to calculate the reversible energy available in thermal systems using second law thermodynamics analysis, as well as a method for assessing and optimizing the TES system's performance. Three systems were analysed and compared as $MgCl_2$ with graphite foam, cascading PCMs of KCl and $MgCl_2$ with graphite foam, and $MgCl_2$ without graphite foam. The technical specifications and the efficiency result are summarized in Table 10. In this study, the cascading PCMs had a slightly better exergy efficiency than the graphite foam-$MgCl_2$ combination, with a difference of about 1%.

Gong and Mujumdar[120] carried out a mathematical simulation to investigate single and different arrangement of composite PCM slab with different melting points and thermophysical properties. At first, the composite slab was supposed to be uniformly at 26°C. At the initiation of the first cycle, the upper face of the slab was maintained at a constant temperature (T_{wm}) at 120°C, which was greater than the fusion temperatures of the PCMs, while the bottom face remained adiabatic. During the freezing phase, the slab's upper face was adiabatic, while the bottom face was maintained at a constant temperature (T_{wm}) at 60°C, which was below the PCMs' fusion temperatures. Several PCMs with melting temperature ranging from 70°C to 105°C were arranged as 2 and 3 of multiple PCMs slab, and subsequently compared with a single PCMs with melting temperature (T_m) of 90°C. It was reported that the highest enhancement was achieved when employing three multiple PCMs slab with melting temperature of 105°C, 90°C, and 75°C, as shown in Case 3 in Table 11. In this case, 21.9% of energy improvement was obtained compared with single PCMs (Case 1).

5 | APPLICATION OF MEDIUM AND HIGH-MELTING TEMPERATURE PCMS

The following sections discuss the utilization of PCMs for high-temperature applications. The application is focused on the capture and storage of thermal energy generated by solar energy and industrial waste heat.

TABLE 10 Exergy efficiency in the latent heat storage system[119]

	Round trip exergy efficiency
Case 1	
Graphite foam–$MgCl_2$	96.80%
8-h charging, inlet temp. 820°C	
Average outlet temp. 765.0°C	
$V_{HTF\_char} = 0.15$ m/s	
12-h discharging, inlet temp. 607°C	
Average outlet temp. 664.0°C	
$V_{HTF\_dis} = 0.15$ m/s	
Case 2	
Cascading PCMs: KCl and $MgCl_2$ (with graphite foam)	97.80%
8-h charging, inlet temp. 820°C	
Average outlet temp. 773.5°C	
$V_{HTF\_char} = 0.15$ m/s	
12-h discharging, inlet temp. 616°C	
Average outlet temp. 664.6°C	
$V_{HTF\_dis} = 0.1$ m/s	
Case 3	
PCM: $MgCl_2$ (without graphite foam)	67.70%
8-h charging, inlet temp. 820°C	
Average outlet temp. 811.9°C	
$V_{HTF\_char} = 0.15$ m/s	
12-h discharging, inlet temp. 578°C	
Average outlet temp.584.1°C	
$V_{HTF\_dis} = 0.1$ m/s	

Note: Reused with permission from Elsevier license number 5184400297418.

5.1 | PCM in solar energy

Regardless of the abundance of solar energy, the application based on solar energy resource is limited due to its fluctuant occurrence. Therefore, the needs of PCM as TES will reduce and overcome this shortcoming. The integration of solar energy abundance with PCM is carried out for a variety of applications, including solar power generation and solar cookers.

5.1.1 | Solar power generation

Concerning to the application of PCM for solar power generation, first reference is exemplified by Laing et al[121,122] who studied the use of thermal energy storage (TES) in solar thermal power plants with direct steam generator (DSG) system. The TES consisted of sensible

TABLE 11 Energy enhancement of multiple 3-PCMs[120]

Case	Temperature (°C)	Energy charge-discharge, Q_T (J/m^2)	Ratio of actual energy with maximum energy, Q_T/Q_M	Enhancement (%)
1	$T_{wm} = 120$ $T_m = 90$ $T_{wf} = 60$	404 508	0.632	—
2	$T_{wm} = 120$ $T_{m1} = 90$ $T_{m2} = 90$ $T_{m3} = 90$ $T_{wf} = 60$	489 753	0.765	21.1
3	$T_{wm} = 120$ $T_{m1} = 105$ $T_{m2} = 90$ $T_{m3} = 75$ $T_{wf} = 60$	493 178	0.771	21.9
4	$T_{wm} = 120$ $T_{m1} = 110$ $T_{m2} = 90$ $T_{m3} = 70$ $T_{wf} = 60$	466 976	0.73	15.4

Note: Reused with permission from Elsevier license number 5184400487474.

heat for pre-heating and superheating, while latent heat was used for the evaporator. Sodium nitrate ($NaNO_3$) with a melting temperature of 306°C was selected as PCM. A laboratory-scale test was conducted on 140 kg $NaNO_3$ and tested for more than 4000 hours and resulted in 172 melting/solidification cycles without degradation. However, $NaNO_3$ worked on different melting and solidification temperatures that directly related to operating pressure and impacted the DSG design. Therefore, high-pressure steam was throttled to mix the steam generated in the solar field and steam generated in the storage. Due to this barrier, Birnbaum et al[123] proposed a reheat based on a steam-steam heat exchanger for the low-pressure turbine by utilizing a second PCM, KNO_3, as the thermal energy storage.

Due to the varying pressure levels during PCM discharging process in DSG, Laing et al[124] examined sliding pressure operation in three different modes: forced circulation, natural circulation and once-through operation. In the scenario of forced circulation, the mass flow rate was set by a pump. In the case of natural circulation, the difference in density between the water column in the cycle's steam drum line and the two-phase water column inside the storage tubes compelled the flow. They measured the temperature of PCM at different positions, hot and cold temperature of HTF, water/steam mass flow rate through PCM (mDCh), and steam production (mSteam). It was observed the longer discharge time of once-through operation by about 23% and 18.5% compared with the forced and natural circulation, respectively. This finding revealed that the prospective and practical once-through mode might eliminate either the recirculation pump or the full circulation cycle, including the steam drum, which potentially resulted in cost reduction.

Feldhoff et al[125] conducted a comparison analysis between PCM-DSG and a system utilizing parabolic synthetic oil through power plants as HTF, which included an integrated salt-based TES. A parameter of levelised electricity cost (LEC) was used to compare those two systems. LEC was defined as the ratio of the total annual plant costs to the yearly net electricity production. Interestingly, the LEC was observed to PCM-DSG plant achieved about 5.9% to 6.3% higher than the oil reference plant due to the immatureness of the PCM system. Using PCM storage for evaporation and pre-heating was recommended to reduce the TES cost.

Bhagat and Saha[126] evaluated numerically the transient response of encapsulated organic PCM A164 with melting temperature of 171°C for solar thermal power plant using hytherm 600 as heat transfer fluid (HTF). A numerical model was developed during melting and

solidification process to measure several key parameters, and it was reported that the temperature and mass rate of HTF provided a positive impact on the heat storage system, but not in the dimensions and porosity of the heat storage system. Another important finding was that the diameter reduction of encapsulated PCM managed well the temperature fluctuation of HTF.

Mehrpooya et al[127] performed a numerical evaluation of an Iranian steam power plant with two regenerative boilers. Integrated solar disc collector and PCMs storage system was designed to take the place of one of the existing regenerative boilers. The composite NaBr (45% wt) and $MgBr_2$ (55%) was selected as PCM with a melting point of 431°C and enthalpy of 212 kJ/kg. Despite a slight reduction in energy efficiency, the hybrid system was able to increase energy efficiency from 38.6% to 41.76% when compared with the two regenerative boilers. The proposed system was also capable of reducing CO_2 emissions by 14.86% corresponding with saving of fuel-natural gas about 8.5 ton/hour.

5.1.2 | Integrated PCM solar cookers

The utilization of conventional solar cookers is limited due to its disability to serve the cooking process during cloudy days or in the late evening. The introduction of PCM will improve the reliability of solar cookers by storing solar energy on bright days and releasing it later in the evening.

Box-type solar cooker with inner reflectors was carried out experimentally by Domanski et al[128] during the charging and discharging of PCMs. A storage-cooking vessel (SCV) consisted of two concentric cylindrical vessels with a gap between the outer and inner walls where PCM was located. They selected 1.1 kg stearic acid (SA) ($T_m = 67 - 69°C$) and 2 kg magnesium nitrate hexahydrate (MNHH) ($T_m = 89°C$) as PCMs and ten calibrated K-type thermocouples (TC) were attached at various points. Using solar simulator, SCV with an empty or water loaded cooking medium was used to begin the melting investigations. When TCs in PCM reached around the same temperature which was higher than the PCM's melting point, a melting experiment was accomplished. The sun simulator was then switched off and the solidification experiment was initiated at a preset starting temperature soon after the melting experiment was complete, with known water mass as a cooking fluid. The highest thermal efficiency was achieved by about 82.4% during solidification of MNHH for heating 1.4 kg of water as cooking load from 20.3 until 75°C for 75 minutes. This value was approximately 3 to 4 times higher than in steam and heat pipe solar cookers for indoor cooking. To accomplish high-temperature cooking, they suggested PCMs with high melting temperatures, such as magnesium chloride hexahydrate ($MgCl_2 \cdot H_2O$).

Sharma et al[129] designed a cooking vessel that consisted of 8 cm height of two-concentric cylinder with a diameter of 18 and 25 cm in a box-type solar cooker. Two kilograms of commercial-grade acetamide ($T_m = 82°C$) was selected as LHS material, and filled the gap between the cylinders. The cooking investigations were carried out by comparing the "PCM Cooker" to the "Reference Cooker" without PCM using the same amount of rice and water as cooking load. The experiments were conducted in three batches a day during the summertime, while two batches in winter season in India. They reported that during the summer season, the "PCM Cooker" allowed for the cooking of three batches each day at 11 A.M., 4 P.M., and 6 P.M. In the "Reference Cooker" however, evening cooking could not be done. Meanwhile, in winter period, the "PCM Cooker" allowed two bats of cooking at 9.50 A.M. and 3.30 P.M., while in "Reference Cooker" the load could only be cooked for one batch only. Additionally, it was stated that if a PCM with melting point between 105°C and 110°C was employed, cooking with the same design was potentially conducted at night.

Furthermore, Buddhi et al[130] continued to develop a two-concentric cylinder in a larger size with 12.5 cm of height and two concentric aluminium cylinders with diameter 20 and 30 cm. Acetanilide ($T_m = 118.9°C, \Delta h_m = 222\,J/g$) was utilized as LHS material and filled the gap between the cylinders. The cooking experiment was conducted at evening during winter season using rice and water as cooking load at varying mass. Initially, 2.25 kg of acetanilide was exposed to the sun between 10 A.M. and 5 P.M. using a single existing reflector. Cooker with 0.50 kg of food (0.15 kg rice and 0.35 kg water) was subsequently loaded to the storage unit and well cooked after 3 hours. On the next day, the same cooking load was placed into the cooker half an hour later than the previous day, and after 2 hours, it was discovered to be properly cooked. However, when cooking began at 6 p.m., the meal was undercooked. Following that, the cooking method was enhanced by utilizing 4 kg of acetanilide and three reflectors to accomplish evening cooking at 6 p.m. with the same food quantity. Surprisingly, the improved solar cooker was capable of cooking 0.40 kg rice and 1.2 kg water at 09.30 p.m. in about 2 hours.

Coccia et al[131] developed and assessed a portable solar box cooker with a reflective mirror in the upper part to direct solar radiation to the cooking chamber through a glass cover. It was designed to build the cooker with a 4.08-times larger cooker aperture surface compared with the surface area of the glass cover. Two concentric

cylindricals were placed in the chamber as cooking pot, and erythritol filled the annulus between those pots. To observe the effect of PCM in solar cooker, silicone oil was utilized as cooking load with and without the presence of erythritol. In the absence of solar radiation, it was discovered that the system with PCM was capable to cool silicone oil from 125°C to 100°C about 4.51 times longer than that of silicon oil alone.

Chaudhary et al[132] examined the improvement of solar cooker based on parabolic dish collector for evening cooking in Indian climatic conditions by using acetanilide as LHS. The cooking vessel was focused by solar radiation by setting it at the focal point of the solar parabolic dish collector, as shown in Figure 14. The solar cooker was constructed from two hollow concentric cylinders separated by a gap filled with PCM. The cooking vessel was exposed to solar radiation for 7 hours from morning to noon, prior to heat the water as cooking load in an insulator box from 4 to 8 P.M. To enhance the thermal performance of cooking system, the solar cooker surface was painted in black, including the painted black surface along the glazing. They discovered that the maximum temperature of the cooking medium achieved during the cooking process was 52.2°C in the case of an ordinary solar cooker, 84.3°C in the case of blackened surfaces of solar cooker, and 88.4°C in the case of a glazed darkened surfaces of solar cooker. These studies indicated that blackened surfaces and glazed darkened surfaces conserved approximately 26.8% and 32.3% more heat, respectively, than ordinary solar cooker.

Moreover, Yadav et al[133] continued the use of parabolic dish collector for evening cooking using acetamide as PCM. A pressure cooker was put in the centre of the cooking vessel, which was made up of two concentric pots of different diameters, each holding PCMs in the inner pot and various sensible heat storage materials (SHSMs) in the outer pot. Sand, iron grits, stone pebbles, iron balls were used as SHSMs under same cooking load of 200 g rice and 400 mL water. The system was exposed to solar radiation for 3 hours at noon prior to the evening cooking process in an insulator box for about 4 hours. It was observed that combining acetamide with sand and stone pebbles could reach a maximum temperature of PCM at 83.5°C and 82.9°C, resulting in well-cooked meals by extracting about 70% of stored energy. However, cooking using iron grits and balls as SHSMs was ineffective due to the poor rate of heat transmission of such SHSMs.

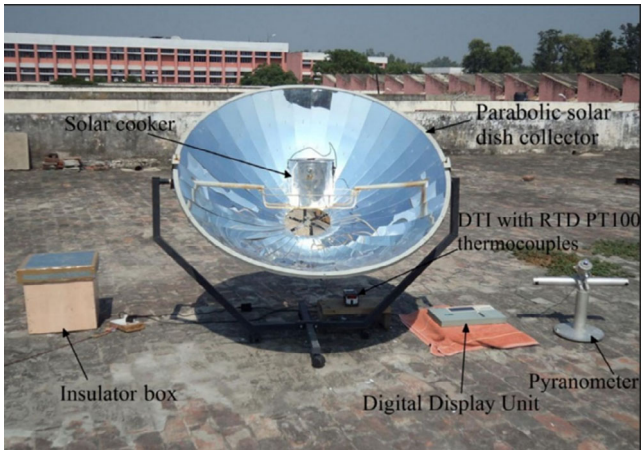

FIGURE 14 Parabolic solar collector.[132] Reused with permission from AIP Publishing license number 5238470307435

Bhave and Thakare[134] selected magnesium chloride hexahydrate ($MgCl_2{\cdot}H_2O$) ($T_m = 118°C, \Delta h_m = 167\,J/g$) as PCM to be used for paraboloid concentrating cooker. A double-walled cylindrical was used as cooking vessel with 100 mL water and 50 g rice as cooking load. PCMs were encased in 21 tubes and immersed in thermic mineral oil as HTF in the lowest portion of the vessel to minimize incongruent melting of PCMs and to preserve contact with the bottom and sides of the cooking vessel. The charging procedure took 50 minutes at midday to achieve PCM temperature of 135°C before a 30-minute cooking test in an insulated glass wool. Furthermore, they observed that the energy consumption efficiency for this cooking test was around 32.66%, which was equivalent to the cooking utilizing wood burning cookstoves.

Mawire et al[135] assessed the performance of a solar cooker pot employing erythritol as a TES material and compared it to that of sunflower oil as a sensible storage material. Two parabolic dish solar cookers were constructed and tested with varying loads on each of those two storage materials during the sun cooking period. Subsequently, insulated wonderbag was utilized during off-sunshine periods. The experimental results indicated that erythritol took around 1.32 to 2.1 times longer to cook than sunflower oil during the sunny period. However, due to the smaller temperature drop, the erythritol cooking pot outperformed the sunflower oil cooking pot over the storage cooking time. As a result, erythritol cookers had a utilization efficiency that was around 1.1 to 3.86 times that of sunflower oil.

Hussein et al[136] investigated the use of magnesium nitrate hexahydrate as PCM in an indirect solar cooker that consisted of an exterior flat-plate solar collector linked to an indoor PCM cooking unit through a closed-loop wickless heat pipes network. Two plane reflectors were installed on the outdoor collector's top and bottom edges to increase the amount of solar radiation falling on it. Two cooking pots with a volume of 3 and 4 L were built and PCM was filled in the space between the pots in the inner box. The cooking experiment was carried out in

Egypt during the summer and initially tested without cooking load for 48 hours, and resulted in the lowest PCM temperature as 76°C on 9 A.M. on the second day. This was slightly higher than the required temperature for cooking most types of meals. Different amount of water was subsequently heated for 24 hours from 6 A.M. to 6 A.M. the next day, and the temperatures of the water load within the two cooking pots exceeded 80°C during the test period from 1 PM until late evening. It was, nevertheless, insufficient for culinary cooking in the next early morning. Finally, different cooking loads were conducted for 3 batches for 24 hours and the results were recorded. A well-cooked meal was acquired for lunch and supper during the first and second batches, respectively. Meanwhile, the third batch was used to keep the food warm for the next morning's breakfast.

Another indirect solar cooker was studied by Sharma et al[137] by employing 45 kg erythritol as a LHS material under Japanese climatic conditions during summer and winter season. Solar thermal energy was collected outdoors using evacuated tube solar collectors (ETSC) and transmitted via water HTF to a PCM storage unit. Cooking vessel was put inside PCM storage unit using various amount of water as cooking load. It was claimed that throughout the summer, the temperature of PCM was between 112°C to 128°C, which enabled it to boil the water to a temperature more than 95°C at midday and evening. They also reported that night-time cooking was faster than noon cooking for the same load. Additionally, it was stated that PCM temperatures near 100°C were detected in the early morning, which was potentially utilized to keep heated water warm till the next morning. However, throughout the winter, low-temperature cooking near 75°C happened, indicating that the PCM did not entirely melt, despite the fact that certain meals could still be cooked.

5.2 | Waste heat recovery applications

Industrial waste heat (IWH) is identified as an available resource of thermal energy that can be recovered and stored in PCMs for later application. This chapter reviews some of the past PCM systems which have been considered for industrial waste heat recovery application.

Merlin et al[138] demonstrated experimentally the use of composed paraffin RT82 ($T_m = 82.5°C - 88°C$) with expanded natural graphite (ENG) for waste heat recovery in the sterilization process of the food industry. The composite PCM and ENG were installed in a secondary loop for heating and cooling purposes utilizing water HTF. Initially, the composite LHS was employed for preheating process to replace the steam boiler. The conventional vapour system took over when the temperature of HTF in the secondary loop approached the melting point of composite PCM. During the cooling step, the PCM was used to chill the sterilizing water until it was entirely melted before being cooled by tap water. The results indicated that the storage system was able to conserve 6 kWh, or 15% of the energy used in the process, and delivered thermal power more than 100 kW. For further enhancement, they advised that more PCMs with graded phase change temperatures be used to cover a greater amount of recovered energy.

Kaizawa et al[139] examined the melting and solidification of 80 kg erythritol in a trans-heat (TH) system of waste heat transportation. By melting the PCMs using circulated heat transfer oil (HTO) in a direct heat exchanger, IWH was stored as latent heat. The stored heat in PCM was then transported across a large region by a container vehicle up to 35 km from the heat source. Finally, the heat was distributed to business buildings, hospitals, and hotels, among other locations. It was found that the HTO flow rate was obviously controlling the charging of the PCM. It took 8 hours to completely melt the PCM, which was equal to storing 51.7 MJ of heat at a temperature above 135°C at a 10 nL/minute HTO flow rate. Heat transmission was, however, abruptly terminated during heat discharging because PCM solidification prevented HTO flow at 4.2 and 10.0 nL/min, which accounted for about 70% of heat release.

Nomura et al[56] continued to study the feasibility of a waste-heat transportation (HT) system using the binary eutectic mixture Na_2CO_3/NaOH ($T_m = 285°C, \Delta h_m = 252\,J/g$) and dibenzyltoluene as HTF. The HT system was compared with conventional system using combustion heat of fossil fuels without transportation. The feasibility was subsequently evaluated based on energy requirements, exergy loss, and CO_2 emissions. It was reported that the waste HT system supplied the heat of 7.00 GJ/1 cycle at 250°C, which resulted in considerably lower energy demands, exergy losses, and CO_2 emissions by about 9.5%, 39.7%, and 19.6%, respectively, compared with the conventional system.

Furthermore, Nomura et al[140] proposed the use of NaOH ($T_m = 320°C, \Delta h_m = 159\,J/g$) as PCM and oil as HTF to recover and transport high-temperature waste heat from steelworks to a chemical plant. The HT system using latent heat (LHT) was compared with an oil sensible heat transportation (SHT) system and a conventional system that used fuel for combustion heat. Due to the high latent heat capacity of PCM, results revealed that the LHT system supplied 2.76 times more of energy than the SHT system. Additionally, the LHT system consumed less energy, had fewer exergy losses, and produced less CO_2 than the SHT system by roughly 47.05%, 31.25%, and 43.89%, respectively, with corresponding 91.42%, 62.06%, and 81.25% that of conventional system.

Koide et al[141] researched and evaluated the efficacy of packed bed employing pellets within MEPCM, which was envisioned for use in waste heat recovery from electric furnace. The MEPCM was prepared as fabricated in Reference 77 using alloy Al-25 % Si at melting point of 577°C. A 1 L-scale cylindrical packed bed heat exchanger was filled in by MEPCM and tested at various airflow rates ranging from 75 to 150 L/min. The heat exchange efficiency was defined as the ratio of experimental to the maximum theoretical value of heat storage/release amount of MEPCM. Despite the supercooling effect, the heat exchanger operated effectively, achieving an efficiency of more than 90% when the air flow rate exceeded 125 L/min. Additionally, the research of laminar or turbulent flow was proposed to enhance the accuracy of the MEPCM composite heat exchanger.

Nardin et al[142] proposed the use of aluminium ($T_m = 660°C, \Delta h_m = 396\,J/g$) as PCM to reduce the temperature fluctuation from electric arc furnaces in steel industry. Off-gas forced the PCM to reach temperatures over its melting point during the process at high temperatures, leading in a transition from the solid to the liquid state and the accumulation of latent heat of fusion. At low temperatures, off-gas led the PCM to transition from liquid to solid state, releasing the latent heat of solidification. Results revealed that the profile of off-gas was significantly smoothed by PCM. They calculated that if the recovery system was installed, it would generate a net electrical power of around 6 MWe, saving approximately 14.4% of electrical energy supply.

Moreover, Magro et al[143] evaluated the using PCM with melting temperature of 576°C for temperature smoothing due to the high power fluctuation of the organic Rankine cycle (ORC) from the waste heat of billet reheating furnace in the steel industry. The eutectic alloy Al-12%wt Si, which had latent heat of fusion 560 kJ/ kg, was selected as PCM and integrated with billet reheating furnace, as shown in Figure 15. The capacity factor (CF), load factor, and thermal efficiency of the system without PCM were utilized as comparison parameters. The capacity factor (CF) was defined as the quantitative relationship between the amount of electricity generated and the greatest amount of electricity that could be produced, whereas the load factor was defined as the ratio of real thermal power recovered to its design value. The PCM-based technology enabled the ORC system to run continuously above the minimum thermal power which was denoted by red dot line, whereas the existing ORC system ran for the majority of the time below the minimum thermal power in the present waste heat recovery system. Additionally, with the introduction of PCM-based technology, the ORC system operated continuously in its high-efficiency zone with load factor more than 0.5, whereas the ORC system in the current waste heat recovery system operated in the low-efficiency zone for more than 67% of the total working time. These findings correlated with an improvement in CF from 38% to 52% and an increase in thermal efficiency from 15.5% to 16.4% as a result of the adoption of PCM-based technology.

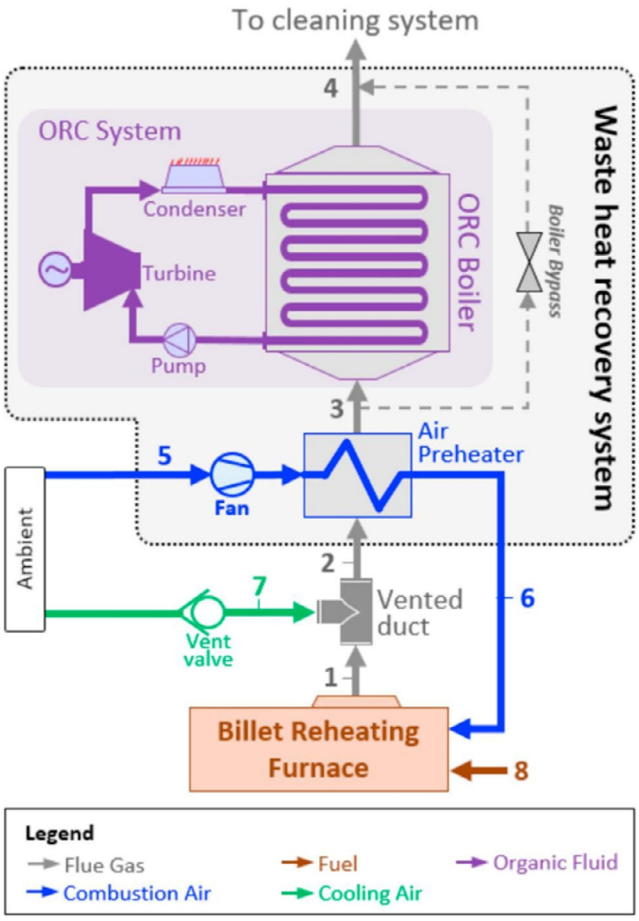

FIGURE 15 The integration of PCM for waste heat recovery from billet reheating furnace.[143] Reused with permission from Elsevier license number 5260860214017

6 | CONCLUSION

This paper primarily discusses microencapsulation techniques, thermal performance improvement, and the use of PCMs with a medium or high melting point.

This review established that a variety of PCMs with a medium to high melting point are commercially microencapsulated and employed in a variety of applications. Inorganic and paraffin PCMs are commonly encapsulated for medium melting temperature. Meanwhile, salt-based, metallic, inorganic compound, and the eutectic are extensively encapsulated and utilized for high-

temperature applications. Each type of PCM has its characteristics. For instance, metallic-based PCMs are characterized based on their high melting temperature, high thermal conductivity, and high latent heat. However, they suffer from corrosiveness which limits their applications. Salt-based PCMs have been widely investigated and applied for medium and high application due to their high latent heat and relatively cheaper than those of metal-based PCMs. Nevertheless, low thermal conductivity, phase separation, and supercooling confine their competitiveness. Eutectic PCMs are attractive due to their adjustable thermophysical properties by mixing different types of PCM. Regardless of complexity, they are capable of high thermal conductivity and relatively high latent heat.

Due to chemical corrosion and thermal stress during phase transition, the shell material selection is also crucial when encapsulating PCMs with a medium or high melting point. Inorganic shell is required with temperature degradation above the high-melting temperature of the PCM such as silica-based and ceramic, which is widely developed through sol-gel and hydrothermal encapsulation method. However, the encapsulation through hydrothermal followed by heat oxidation is limited for encapsulating particular PCMs with Al_2O_3 shell. Several polymer shell materials are also utilized by some studies to encapsulate high-temperature PCMs, such as polyurethane, poly(methyl methacrylate) (PMMA), poly(styrene-butyl acrylate) (PSBA), and poly(ethyl-2-cyanoacrylate) (PECA) by chemical techniques. However, polymerization with salt-based PCMs needs more attention compared with paraffin PCMs caused by their hydrophilicity nature and water content during phase transition. Additionally, it is discovered that void creation during microencapsulation is critical for allowing volume expansion during phase transition, resulting in increased thermal stability.

This paper also reviews the thermal performance enhancement employed in medium and high-melting temperature PCMs, such as additive-composited PCM and multiple PCMs. Metal, carbon, and ceramic-based have been commonly introduced with PCM for thermal performance improvement. Ceramic material to encapsulate corrosive PCM of metal and alloy has been reported to overcome its corrosion issue. Compared with metal-based, carbon materials are potentially used due to their non-corrosive characterization, light weight, and lower density, which are not owned by metal-based materials. Various combinations of multiple PCMs are also developed by numerous studies to improve the energy efficiency compared with single PCM. Therefore, the selection of PCMs and their proportion play important role in the thermal performance.

Solar energy generation is one of the PCM-solar applications that require the greatest melting temperature range of PCM, around 100°C to 700°C. The most often used PCMs in solar energy generation are inorganic compounds such as sodium nitrate and potassium nitrate. Meanwhile, organic non-paraffin and salt hydrate PCM with melting points of 80°C to 120°C, such as acetamide, acetanilide, or MNHH, are required for the solar cooking system. Additionally, salt hydrate and eutectic PCM with a melting point greater than 200°C are the most often utilized materials for industrial heat recovery. In general, salt hydrate, organic non-paraffin, and eutectic PCM are typically used for high-temperature applications.

Finally, the review exhibits that medium- and high-melting temperature PCM requires more research studies to be more significant in the future.

ACKNOWLEDGEMENT

The authors would like to thank the Indonesia Ministry of Education and Culture (Kementerian Pendidikan dan Kebudayaan), Directorate General of Resources for Science Technology and Higher Education, for funding this research through Beasiswa Pendidikan Pascasarjana Luar Negeri (BPPLN) scholarship Grant No: T/978/D3.2/KD.02.01/2019.

DATA AVAILABILITY STATEMENT

The data used to support the findings of this study are included in the article.

ORCID

Rizal Sinaga https://orcid.org/0000-0002-8501-0958

REFERENCES

1. Avtar R, Tripathi S, Aggarwal AK, Kumar P. Population-urbanization-energy nexus: a review. *Resources*. 2019;8:1-21. doi:10.3390/resources8030136
2. Osobajo OA, Otitoju A, Otitoju MA, Oke A. The impact of energy consumption and economic growth on carbon dioxide emissions. *Sustainability*. 2020;12:1-16. doi:10.3390/SU12197965
3. Lamb WF, Wiedmann T, Pongratz J, et al. A review of trends and drivers of greenhouse gas emissions by sector from 1990 to 2018. *Environ Res Lett*. 2021;16:073005. doi:10.1088/1748-9326/abee4e
4. Gielen D, Boshell F, Saygin D, Bazilian MD, Wagner N, Gorini R. The role of renewable energy in the global energy transformation. *Energy Strat Rev*. 2019;24:38-50. doi:10.1016/j.esr.2019.01.006
5. International Energy Agency. *Solar Energy Perspectives*. Vol 1. Luxembourg: OECD Publishing; 2011. doi:10.1787/9789264124585-en
6. Papapetrou M, Kosmadakis G, Cipollina A, La Commare U, Micale G. Industrial waste heat: estimation of the technically available resource in the EU per industrial sector, temperature level and country. *Appl Therm Eng*. 2018;138:207-216. doi:10.1016/j.applthermaleng.2018.04.043

7. Fallahi A, Guldentops G, Tao M, Granados-Focil S, Van Dessel S. Review on solid-solid phase change materials for thermal energy storage: molecular structure and thermal properties. *Appl Therm Eng*. 2017;127:1427-1441. doi:10.1016/j.applthermaleng.2017.08.161
8. Su W, Darkwa J, Kokogiannakis G. Review of solid-liquid phase change materials and their encapsulation technologies. *Renew Sustain Energy Rev*. 2015;48:373-391. doi:10.1016/j.rser.2015.04.044
9. Huang X, Zhu C, Lin Y, Fang G. Thermal properties and applications of microencapsulated PCM for thermal energy storage: a review. *Appl Therm Eng*. 2019;147:841-855. doi:10.1016/j.applthermaleng.2018.11.007
10. Li Q, Ma X, Zhang X, Ma J, Hu X, Lan Y. Microencapsulation of Al-Zn alloy as phase change materials for high-temperature thermal storage application. *Mater Lett*. 2022;308:131208. doi:10.1016/j.matlet.2021.131208
11. Zhang G, Li J, Chen Y, et al. Encapsulation of copper-based phase change materials for high temperature thermal energy storage. *Sol Energy Mater Sol Cells*. 2014;128:131-137. doi:10.1016/j.solmat.2014.05.012
12. Wu X, Fan M, Cui S, Tan G, Shen X. Novel Na2SO4@SiO2 phase change material with core-shell structures for high temperature thermal storage. *Sol Energy Mater Sol Cells*. 2018;178:280-288. doi:10.1016/j.solmat.2018.01.030
13. Leng G, Qiao G, Jiang Z, et al. Microencapsulated & form-stable phase change materials for high temperature thermal energy storage. *Appl Energy*. 2018;217:212-220. doi:10.1016/j.apenergy.2018.02.064
14. Fuensanta M, Paiphansiri U, Romero-Sánchez MD, Guillem C, López-Buendía ÁM, Landfester K. Thermal properties of a novel nanoencapsulated phase change material for thermal energy storage. *Thermochim Acta*. 2013;565:95-101. doi:10.1016/j.tca.2013.04.028
15. Wei H, Wang C, Yang S, et al. A strategy for designing microencapsulated composite phase change thermal storage materials with tunable melting temperature. *Sol Energy Mater Sol Cells*. 2019;203:110166. doi:10.1016/j.solmat.2019.110166
16. Lin Y, Jia Y, Alva G, Fang G. Review on thermal conductivity enhancement, thermal properties and applications of phase change materials in thermal energy storage. *Renew Sustain Energy Rev*. 2018;82:2730-2742. doi:10.1016/j.rser.2017.10.002
17. Xu B, Li P, Chan C. Application of phase change materials for thermal energy storage in concentrated solar thermal power plants: a review to recent developments. *Appl Energy*. 2015;160:286-307. doi:10.1016/j.apenergy.2015.09.016
18. Herez A, Ramadan M, Khaled M. Review on solar cooker systems: economic and environmental study for different Lebanese scenarios. *Renew Sustain Energy Rev*. 2018;81:421-432. doi:10.1016/j.rser.2017.08.021
19. Sharif MKA, Al-Abidi AA, Mat S, et al. Review of the application of phase change material for heating and domestic hot water systems. *Renew Sustain Energy Rev*. 2015;42:557-568. doi:10.1016/j.rser.2014.09.034
20. Zhou C, Wu S. Medium- and high-temperature latent heat thermal energy storage: material database, system review, and corrosivity assessment. *Int J Energy Res*. 2019;43:621-661. doi:10.1002/er.4216
21. Liu M, Saman W, Bruno F. Review on storage materials and thermal performance enhancement techniques for high temperature phase change thermal storage systems. *Renew Sustain Energy Rev*. 2012;16:2118-2132. doi:10.1016/j.rser.2012.01.020
22. Costa SC, Kenisarin M. A review of metallic materials for latent heat thermal energy storage: Thermophysical properties, applications, and challenges. *Renew Sustain Energy Rev*. 2022;154:111812. doi:10.1016/j.rser.2021.111812
23. Liu M, Omaraa ES, Qi J, et al. Review and characterisation of high-temperature phase change material candidates between 500 C and 700°C. *Renew Sustain Energy Rev*. 2021;150:111528. doi:10.1016/j.rser.2021.111528
24. Milián YE, Gutiérrez A, Grágeda M, Ushak S. A review on encapsulation techniques for inorganic phase change materials and the influence on their thermophysical properties. *Renew Sustain Energy Rev*. 2017;73:983-999. doi:10.1016/j.rser.2017.01.159
25. Pereira da Cunha J, Eames P. Thermal energy storage for low and medium temperature applications using phase change materials - a review. *Appl Energy*. 2016;177:227-238. doi:10.1016/j.apenergy.2016.05.097
26. Liu H, Wang X, Wu D. Innovative design of microencapsulated phase change materials for thermal energy storage and versatile applications: a review. *Sustain Energy Fuels*. 2019;3:1091-1149. doi:10.1039/c9se00019d
27. Zhu S, Nguyen MT, Yonezawa T. Micro- and nano-encapsulated metal and alloy-based phase-change materials for thermal energy storage. *Nanoscale Adv*. 2021;3:4626-4645. doi:10.1039/d0na01008a
28. Iqbal K, Khan A, Sun D, et al. Phase change materials, their synthesis and application in textiles—a review. *J Text Inst*. 2019;110:625-638. doi:10.1080/00405000.2018.1548088
29. Zhao CY, Zhang GH. Review on microencapsulated phase change materials (MEPCMs): fabrication, characterization and applications. *Renew Sustain Energy Rev*. 2011;15:3813-3832. doi:10.1016/j.rser.2011.07.019
30. Hassan A, Laghari MS, Rashid Y. Micro-encapsulated phase change materials: a review of encapsulation, safety and thermal characteristics. *Sustainability*. 2016;8:1046. doi:10.3390/su8101046
31. Kenisarin M, Mahkamov K. Solar energy storage using phase change materials. *Renew Sustain Energy Rev*. 2007;11:1913-1965. doi:10.1016/j.rser.2006.05.005
32. Rubitherm PCM. Rubitherm Technol; 2015. http://www.rubitherm.com/english/index.htm. Accessed April 20, 2020.
33. Mehling H, Cabeza LF. *Heat and Cold Storage with PCM: An up to Date Introduction Into Basics and Applications*. Berlin: Springer; 2008. doi:10.1007/978-3-540-68557-9
34. Kosny J. *PCM-Enhanced Building Components: an Application of Phase Change Materials in Building Envelopes and Internal Structures*. Manchester, UK: Springer International Publishing; 2015. doi:10.1007/978-3-319-14286-9
35. Yan Q, Liang C. The thermal storage performance of monobasic, binary and triatomic polyalcohols systems. *Sol Energy*. 2008;82:656-662. doi:10.1016/j.solener.2007.12.008
36. Lingayat AB, Suple YR. Review on phase change material as thermal energy storage medium: materials. *Appl Int J Eng Res Appl*. 2013;3:916-921.

37. Sharma A, Tyagi VV, Chen CR, Buddhi D. Review on thermal energy storage with phase change materials and applications. *Renew Sustain Energy Rev*. 2009;13:318-345. doi:10.1016/j.rser.2007.10.005
38. Sharma SD, Kitano H, Sagara K. Phase change materials for low temperature solar thermal applications. *Res Rep Fac Eng Mie Univ*. 2004;29:31-64.
39. Kerridge DH. The chemistry of molten acetamide and acetamide complexes. *Chem Soc Rev*. 1988;17:181-227. doi:10.1039/CS9881700181
40. Şahan N, Nigon D, Mantell SC, Davidson JH, Paksoy H. Encapsulation of stearic acid with different PMMA-hybrid shell materials for thermotropic materials. *Sol Energy*. 2019;184:466-476. doi:10.1016/j.solener.2019.04.026
41. Karaipekli A, Sari A, Kaygusuz K. Thermal conductivity improvement of stearic acid using expanded graphite and carbon fiber for energy storage applications. *Renew Energy*. 2007;32:2201-2210. doi:10.1016/j.renene.2006.11.011
42. Gunasekara SN, Ignatowicz M, Chiu JNW, Martin V. Thermal conductivity measurement of erythritol, xylitol, and their blends for phase change material design: a methodological study. *Int J Energy Res*. 2019;43:1785-1801. doi:10.1002/er.4403
43. Kim H, Kim K, Kim H, Lee DJ, Park J. Eco-friendly synthesis of water-glass-based silica aerogels via catechol-based modifier. *Nanomaterials*. 2020;10:1-10. doi:10.3390/nano10122406
44. Magon P, Bhagyalakshmi P, Rajan K. Experimental study on phase change material in low thermal application. *Int J Appl Eng Res*. 2015;10:970-974.
45. Sun T, Teja AS. Density, viscosity, and thermal conductivity of aqueous benzoic acid mixtures between 375 K and 465 K. *J Chem Eng Data*. 2004;49:1843-1846. doi:10.1021/je0497247
46. Krishna Bama G, Anitha R, Ramachandran K. On the thermal properties of aqueous solution of D-mannitol. *Nondestruct Test Eval*. 2010;25:67-75. doi:10.1080/10589750902994407
47. Tingting Q, Jinhong L, Xin M, Weimin G, Yong D, Lei N. Enhanced thermal conductivity of PEG/diatomite shape-stabilized phase change materials with Ag nanoparticles for thermal energy storage. *J Mater Chem A*. 2015;3:8526-8536. doi:10.1039/x0xx00000x
48. Mohamad AT, Che Sidik NA. Nano-enhanced phase change material effects on the supercooling degree improvement: a review. *IOP Conf Ser Mater Sci Eng*. 2019;469:012036. doi:10.1088/1757-899X/469/1/012036
49. Khan Z, Khan Z, Ghafoor A. A review of performance enhancement of PCM based latent heat storage system within the context of materials, thermal stability and compatibility. *Energy Conver Manag*. 2016;115:132-158. doi:10.1016/j.enconman.2016.02.045
50. Zalba B, Marin JM, Cabeza LF, Mehling H. Review on thermal energy storage with phase change: materials, heat transfer analysis and applications. 2003;23:251-283. doi:10.1016/S1359-4311(02)00192-8
51. Peng G, Dou G, Hu Y, Sun Y, Chen Z. Phase change material (PCM) microcapsules for thermal energy storage. *Adv Polym Technol*. 2020;2020:9490873. doi:10.1155/2020/9490873
52. Yaws CL. *Thermal Conductivity of Liquid-Inorganic Compounds*. Vol 1274. Norwich, NY: William Andrew Inc; 2009. doi:10.1016/B978-0-8155-2039-9.50013-2
53. Tudor AI, Motoc AM, Ciobota CF, Ciobota DN, Piticescu RR, Romero-Sanchez MD. Solvothermal method as a green chemistry solution for micro-encapsulation of phase change materials for high temperature thermal energy storage. *Manuf Rev*. 2018;5:4. doi:10.1051/mfreview/2018004
54. Ge H, Li H, Mei S, Liu J. Low melting point liquid metal as a new class of phase change material: an emerging frontier in energy area. *Renew Sustain Energy Rev*. 2013;21:331-346. doi:10.1016/j.rser.2013.01.008
55. Kenisarin MM. High-temperature phase change materials for thermal energy storage. *Renew Sustain Energy Rev*. 2010;14:955-970. doi:10.1016/j.rser.2009.11.011
56. Nomura T, Oya T, Okinaka N, Akiyama T. Feasibility of an advanced waste heat transportation system using high-temperature phase change material (PCM). *ISIJ Int*. 2010;50:1326-1332. doi:10.2355/isijinternational.50.1326
57. Gokon N, Jie CS, Nakano Y, et al. Phase change material of copper–germanium alloy as solar latent heat storage at high temperatures. *Front Energy Res*. 2021;9:1-19. doi:10.3389/fenrg.2021.696213
58. Tian H, Wang W, Ding J, Wei X, Huang C. Preparation of binary eutectic chloride/expanded graphite as high-temperature thermal energy storage materials. *Sol Energy Mater Sol Cells*. 2016;149:187-194. doi:10.1016/j.solmat.2015.12.038
59. Cabeza LF, Castell A, Barreneche C, De Gracia A, Fernández AI. Materials used as PCM in thermal energy storage in buildings: a review. *Renew Sustain Energy Rev*. 2011;15:1675-1695. doi:10.1016/j.rser.2010.11.018
60. Al Shannaq R, Farid MM. *Microencapsulation of Phase Change Materials (PCMs) for Thermal Energy Storage Systems*. Vol 1. Sawston, UK: Woodhead Publishing Limited; 2015. doi:10.1533/9781782420965.2.247
61. Ghosh SK. *Functional Coatings: By Polymer Microencapsulation*. Weinheim: Wiley VCH; 2006. doi:10.1002/3527608478
62. Jamekhorshid A, Sadrameli SM, Farid M. A review of microencapsulation methods of phase change materials (PCMs) as a thermal energy storage (TES) medium. *Renew Sustain Energy Rev*. 2014;31:531-542. doi:10.1016/j.rser.2013.12.033
63. Graham M, Shchukina E, De Castro PF, Shchukin D. Nanocapsules containing salt hydrate phase change materials for thermal energy storage. *J Mater Chem A*. 2016;4:16906-16912. doi:10.1039/c6ta06189c
64. Graham M, Coca-Clemente JA, Shchukina E, Shchukin D. Nanoencapsulated crystallohydrate mixtures for advanced thermal energy storage. *J Mater Chem A*. 2017;5:13683-13691. doi:10.1039/c7ta02494k
65. Hayashi Y, Fuchigami K, Taguchi Y, Tanaka M. Preparation of microcapsules containing Erythritol with interfacial Polycondensation reaction by using the (W/O) emulsion. *J Encapsulation Adsorpt Sci*. 2014;04:132-141. doi:10.4236/jeas.2014.44014
66. Zhang H, Balram A, Tiznobaik H, Shin D, Santhanagopalan S. Microencapsulation of molten salt in stable silica shell via a water-limited sol-gel process for high temperature thermal energy storage. *Appl Therm Eng*. 2018;136:268-274. doi:10.1016/j.applthermaleng.2018.02.050
67. Romero-Sanchez MD, Piticescu RR, Motoc AM, Aran-Ais F, Tudor AI. Green chemistry solutions for sol-gel micro-

encapsulation of phase change materials for high-temperature thermal energy storage. *Manuf Rev*. 2018;5:8. doi:10.1051/mfreview/2018003

68. Zhang H, Shin D, Santhanagopalan S. Microencapsulated binary carbonate salt mixture in silica shell with enhanced effective heat capacity for high temperature latent heat storage. *Renew Energy*. 2019;134:1156-1162. doi:10.1016/j.renene.2018.09.011
69. He F, Song G, He X, Sui C, Li M. Structural and phase change characteristics of inorganic microencapsulated core/shell Al–Si/Al2O3 micro-particles during thermal cycling. *Ceram Int*. 2015;41:10689-10696. doi:10.1016/j.ceramint.2015.05.001
70. Alehosseini E, Jafari SM. Micro/nano-encapsulated phase change materials (PCMs) as emerging materials for the food industry. *Trends Food Sci Technol*. 2019;91:116-128. doi:10.1016/j.tifs.2019.07.003
71. Romero-Sanchez MD, Piticescu RR, Motoc AM, Popescu M, Tudor AI. Preparation of microencapsulated KNO3 by solvothermal technology for thermal energy storage. *J Therm Anal Calorim*. 2019;138:1979-1986. doi:10.1007/s10973-019-08825-1
72. Paulo BB, Andreola K, Taranto O, Ferreira AD, Prata AS. Coating approach for a phase change material (PCM). *Powder Technol*. 2019;341:147-156. doi:10.1016/j.powtec.2018.03.003
73. Ushak S, Judith Cruz M, Cabeza LF, Grágeda M. Preparation and characterization of inorganic PCM microcapsules by fluidized bed method. *Materials*. 2016;9:1-11. doi:10.3390/ma9010024
74. Nomura T, Zhu C, Sheng N, Saito G, Akiyama T. Microencapsulation of metal-based phase change material for high-temperature thermal energy storage. *Sci Rep*. 2015;5:1-8. doi:10.1038/srep09117
75. Nomura T, Sheng N, Zhu C, et al. Microencapsulated phase change materials with high heat capacity and high cyclic durability for high-temperature thermal energy storage and transportation. *Appl Energy*. 2017;188:9-18. doi:10.1016/j.apenergy.2016.11.025
76. Nomura T, Yoolerd J, Sheng N, et al. Al/Al_2O_3 core/shell microencapsulated phase change material for high-temperature applications. *Sol Energy Mater Sol Cells*. 2019;193:281-286. doi:10.1016/j.solmat.2018.12.023
77. Sheng N, Zhu C, Saito G, et al. Development of a microencapsulated Al-Si phase change material with high-temperature thermal stability and durability over 3000 cycles. *J Mater Chem A*. 2018;6:18143-18153. doi:10.1039/c8ta04708a
78. Kawaguchi T, Yoolerd J, Sakai H, Shimizu Y, Kurniawan A, Nomura T. Modified preparation of Al2O3@Al microencapsulated phase change material with high durability for high-temperature thermal energy storage over 650 °C. *Sol Energy Mater Sol Cells*. 2022;237:111540. doi:10.1016/j.solmat.2021.111540
79. Sheng N, Zhu C, Sakai H, Akiyama T, Nomura T. Synthesis of Al-25 wt% Si@Al2O3@cu microcapsules as phase change materials for high temperature thermal energy storage. *Sol Energy Mater Sol Cells*. 2019;191:141-147. doi:10.1016/j.solmat.2018.11.013
80. Li Q, Ma X, Zhang X, et al. Preparation of a new capsule phase change material for high temperature thermal energy storage. *J Alloys Compd*. 2021;868:159179. doi:10.1016/j.jallcom.2021.159179
81. Kawaguchi T, Sakai H, Sheng N, Kurniawan A, Nomura T. Microencapsulation of Zn-Al alloy as a new phase change material for middle-high-temperature thermal energy storage applications. *Appl Energy*. 2020;276:115487. doi:10.1016/j.apenergy.2020.115487
82. Li J, Lu W, Luo Z, Zeng Y. Synthesis and thermal properties of novel sodium nitrate microcapsules for high-temperature thermal energy storage. *Sol Energy Mater Sol Cells*. 2017;159:440-446. doi:10.1016/j.solmat.2016.09.051
83. Wei H, Wang C, Yang S, et al. Novel core/void/shell composite phase change materials for high temperature thermal energy storage. *Chem Eng J*. 2020;391:123539. doi:10.1016/j.cej.2019.123539
84. Wei H, Yang S, Wang C, et al. Novel and durable composite phase change thermal energy storage materials with controllable melting temperature. *J Mater Sci Technol*. 2021;86:11-19. doi:10.1016/j.jmst.2020.12.071
85. Li K, Cheng X, Li N, et al. A yolk/shell strategy for designing hybrid phase change materials for heat management in catalytic reactions. *J Mater Chem A*. 2017;5:24232-24246. doi:10.1039/c7ta07147g
86. Bao J, Zou D, Zhu S, Ma Q, Wang Y, Hu Y. A medium-temperature, metal-based, microencapsulated phase change material with a void for thermal expansion. *Chem Eng J*. 2021;415:128965. doi:10.1016/j.cej.2021.128965
87. Ma Q, Zou D, Wang Y, Lei K. Preparation and properties of novel ceramic composites based on microencapsulated phase change materials (MEPCMs) with high thermal stability. *Ceram Int*. 2021;47:24240-24251. doi:10.1016/j.ceramint.2021.05.135
88. Wang K, Zhang T, Wang T, Xu C, Ye F, Liao Z. Microencapsulation of high temperature metallic phase change materials with SiCN shell. *Chem Eng J*. 2022;436:135054. doi:10.1016/j.cej.2022.135054
89. Lopez J, Caceres G, Palomo Del Barrio E, Jomaa W. Confined melting in deformable porous media: a first attempt to explain the graphite/salt composites behaviour. *Int J Heat Mass Transf*. 2010;53:1195-1207. doi:10.1016/j.ijheatmasstransfer.2009.10.025
90. Graham M, Smith J, Bilton M, et al. Highly stable energy capsules with Nano-SiO 2 Pickering Shell for thermal energy storage and release. *ACS Nano*. 2020;14:8894-8901. doi:10.1021/acsnano.0c03706
91. Hong Y, Ding S, Wu W, et al. Enhancing heat capacity of colloidal suspension using nanoscale encapsulated phase-change materials for heat transfer. *ACS Appl Mater Interfaces*. 2010;2:1685-1691. doi:10.1021/am100204b
92. Zhang P, Xiao X, Meng ZN, Li M. Heat transfer characteristics of a molten-salt thermal energy storage unit with and without heat transfer enhancement. *Appl Energy*. 2015;137:758-772. doi:10.1016/j.apenergy.2014.10.004
93. Li Z, Wu ZG. Numerical study on the thermal behavior of phase change materials (PCMs) embedded in porous metal matrix. *Sol Energy*. 2014;99:172-184. doi:10.1016/j.solener.2013.11.017
94. Yang J, Yang L, Xu C, Du X. Numerical analysis on thermal behavior of solid-liquid phase change within copper foam

with varying porosity. *Int J Heat Mass Transf*. 2015;84:1008-1018. doi:10.1016/j.ijheatmasstransfer.2015.01.088

95. Yuan H, Shi Y, Lu C, Xu Z, Ni Y, Lan X. Enhanced performance of high temperature aluminate cementitious materials incorporated with cu powders for thermal energy storage. *Cem Concr Compos*. 2015;55:139-144. doi:10.1016/j.cemconcomp.2014.08.006
96. Benner JZ, Shannon RC, Wu W, Shen L, Metsack AP, Zhao J. The effect of micro-encapsulation on thermal characteristics of metallic phase change materials. *Appl Therm Eng*. 2022;207:118055. doi:10.1016/j.applthermaleng.2022.118055
97. Zhang Z, Zhang N, Peng J, Fang X, Gao X, Fang Y. Preparation and thermal energy storage properties of paraffin/expanded graphite composite phase change material. *Appl Energy*. 2012;91:426-431. doi:10.1016/j.apenergy.2011.10.014
98. Wang T, Wang K, Ye F, Ren Y, Xu C. Characterization and thermal properties of a shape-stable Na2CO3-K2CO3/coal fly ash/expanded graphite composite phase change materials for high-temperature thermal energy storage. *J Energy Storage*. 2021;33:102123. doi:10.1016/j.est.2020.102123
99. Ran X, Wang H, Zhong Y, et al. Thermal properties of eutectic salts/ceramics/expanded graphite composite phase change materials for high-temperature thermal energy storage. *Sol Energy Mater Sol Cells*. 2021;225:111047. doi:10.1016/j.solmat.2021.111047
100. Soleimanpour S, Sadrameli SM, Mousavi SAHS, Jafaripour M. Preparation and characterization of high temperature shape stable NaNO3/diatomite phase change materials with nanoparticles for solar energy storage applications. *J Energy Storage*. 2022;45:103735. doi:10.1016/j.est.2021.103735
101. Kim T, France DM, Yu W, Zhao W, Singh D. Heat transfer analysis of a latent heat thermal energy storage system using graphite foam for concentrated solar power. *Sol Energy*. 2014;103:438-447. doi:10.1016/j.solener.2014.02.038
102. Lan H, Dutta S, Vahedi N, et al. Graphite foam infiltration with mixed chloride salts as PCM for high-temperature latent heat storage applications. *Sol Energy*. 2020;209:505-514. doi:10.1016/j.solener.2020.09.029
103. Singh D, Kim T, Zhao W, Yu W, France DM. Development of graphite foam infiltrated with MgCl2 for a latent heat based thermal energy storage (LHTES) system. *Renew Energy*. 2016;94:660-667. doi:10.1016/j.renene.2016.03.090
104. Zou Q, Zhang Z, Dong Z, et al. Electromagnetic self-encapsulation of carbon fiber reinforced Al matrix composite phase change material for high-temperature thermal energy storage. *J Alloys Compd*. 2022;901:163560. doi:10.1016/j.jallcom.2021.163560
105. Zhong Y, Zhao B, Lin J, et al. Encapsulation of high-temperature inorganic phase change materials using graphite as heat transfer enhancer. *Renew Energy*. 2019;133:240-247. doi:10.1016/j.renene.2018.09.107
106. Zhao YJ, Wang RZ, Wang LW, Yu N. Development of highly conductive KNO3/NaNO3 composite for TES (thermal energy storage). *Energy*. 2014;70:272-277. doi:10.1016/j.energy.2014.03.127
107. Acem Z, Lopez J, Palomo Del Barrio E. KNO3/NaNO3-graphite materials for thermal energy storage at high temperature: part I.-elaboration methods and thermal properties. *Appl Therm Eng*. 2010;30:1580-1585. doi:10.1016/j.applthermaleng.2010.03.013
108. Zhao CY, Wu ZG. Heat transfer enhancement of high temperature thermal energy storage using metal foams and expanded graphite. *Sol Energy Mater Sol Cells*. 2011;95:636-643. doi:10.1016/j.solmat.2010.09.032
109. Wu ZG, Zhao CY. Experimental investigations of porous materials in high temperature thermal energy storage systems. *Sol Energy*. 2011;85:1371-1380. doi:10.1016/j.solener.2011.03.021
110. Gokon N, Nakano D, Inuta S, Kodama T. High-temperature carbonate/MgO composite materials as thermal storage media for double-walled solar reformer tubes. *Sol Energy*. 2008;82:1145-1153. doi:10.1016/j.solener.2008.05.011
111. Ge Z, Ye F, Ding Y. Composite materials for thermal energy storage: enhancing performance through microstructures. *ChemSusChem*. 2014;7:1318-1325. doi:10.1002/cssc.201300878
112. Li Y, Guo B, Huang G, Kubo S, Shu P. Characterization and thermal performance of nitrate mixture/SiC ceramic honeycomb composite phase change materials for thermal energy storage. *Appl Therm Eng*. 2015;81:193-197. doi:10.1016/j.applthermaleng.2015.02.008
113. Wang H, Ran X, Zhong Y, et al. Ternary chloride salt–porous ceramic composite as a high-temperature phase change material. *Energy*. 2022;238:121838. doi:10.1016/j.energy.2021.121838
114. Zhang Y, Wang M, Li J, Wang H, Zhao Y. Improving thermal energy storage and transfer performance in solar energy storage: Nanocomposite synthesized by dispersing nano boron nitride in solar salt. *Sol Energy Mater Sol Cells*. 2021;232:111378. doi:10.1016/j.solmat.2021.111378
115. Peiró G, Gasia J, Miró L, Cabeza LF. Experimental evaluation at pilot plant scale of multiple PCMs (cascaded) vs. single PCM configuration for thermal energy storage. *Renew Energy*. 2015;83:729-736. doi:10.1016/j.renene.2015.05.029
116. Elsanusi OS, Nsofor EC. Melting of multiple PCMs with different arrangements inside a heat exchanger for energy storage. *Appl Therm Eng*. 2020;185:116046. doi:10.1016/j.applthermaleng.2020.116046
117. Wang P, Wang X, Huang Y, Li C, Peng Z, Ding Y. Thermal energy charging behaviour of a heat exchange device with a zigzag plate configuration containing multi-phase-change-materials (m-PCMs). *Appl Energy*. 2015;142:328-336. doi:10.1016/j.apenergy.2014.12.050
118. Michels H, Pitz-Paal R. Cascaded latent heat storage for parabolic trough solar power plants. *Sol Energy*. 2007;81:829-837. doi:10.1016/j.solener.2006.09.008
119. Zhao W, France DM, Yu W, Kim T, Singh D. Phase change material with graphite foam for applications in high-temperature latent heat storage systems of concentrated solar power plants. *Renew Energy*. 2014;69:134-146. doi:10.1016/j.renene.2014.03.031
120. Gong ZX, Mujumdar AS. Enhancement of energy charge-discharge rates in composite slabs of different phase change materials. *Int J Heat Mass Transf*. 1996;39:725-733. doi:10.1016/0017-9310(95)00179-4
121. Laing D, Bahl C, Bauer T, Lehmann D, Steinmann WD. Thermal energy storage for direct steam generation. *Sol Energy*. 2011;85:627-633. doi:10.1016/j.solener.2010.08.015
122. Laing D, Bahl C, Fiß M, et al. Combined storage system developments for direct steam generation in solar thermal power plants. 30th ISES Bienn sol World Congr 2011, SWC 2011; 2011. 1226-37.

123. Birnbaum J, Eck M, Fichtner M, Hirsch T, Lehmann D, Zimmermann G. A direct steam generation solar power plant with integrated thermal storage. *J Sol Energy Eng Trans ASME*. 2010;132:0310141. doi:10.1115/1.4001563
124. Laing D, Bauer T, Breidenbach N, Hachmann B, Johnson M. Development of high temperature phase-change-material storages. *Appl Energy*. 2013;109:497-504. doi:10.1016/j.apenergy.2012.11.063
125. Feldhoff JF, Schmitz K, Eck M, et al. Comparative system analysis of direct steam generation and synthetic oil parabolic trough power plants with integrated thermal storage. *Sol Energy*. 2012;86:520-530. doi:10.1016/j.solener.2011.10.026
126. Bhagat K, Saha SK. Numerical analysis of latent heat thermal energy storage using encapsulated phase change material for solar thermal power plant. *Renew Energy*. 2016;95:323-336. doi:10.1016/j.renene.2016.04.018
127. Mehrpooya M, Ghorbani B, Sadeghzadeh M. Hybrid solar parabolic dish power plant and high-temperature phase change material energy storage system. *Int J Energy Res*. 2019;43:5405-5420. doi:10.1002/er.4637
128. Domanski R, El-Sebaii AA, Jaworski M. Cooking during off-sunshine hours using PCMs as storage media. *Energy*. 1995;20:607-616. doi:10.1016/0360-5442(95)00012-6
129. Sharma SD, Buddhi D, Sawhney RL, Sharma A. Design, development and performance evaluation of a latent heat storage unit for evening cooking in a solar cooker. *Energy Conver Manag*. 2000;41:1497-1508. doi:10.1016/S0196-8904(99)00193-4
130. Buddhi D, Sharma SD, Sharma A. Thermal performance evaluation of a latent heat storage unit for late evening cooking in a solar cooker having three reflectors. *Energy Conver Manag*. 2003;44:809-817. doi:10.1016/S0196-8904(02)00106-1
131. Coccia G, Aquilanti A, Tomassetti S, Comodi G, Di Nicola G. Design, realization, and tests of a portable solar box cooker coupled with an erythritol-based PCM thermal energy storage. *Sol Energy*. 2020;201:530-540. doi:10.1016/j.solener.2020.03.031
132. Chaudhary A, Kumar A, Yadav A. Experimental investigation of a solar cooker based on parabolic dish collector with phase change thermal storage unit in Indian climatic conditions. *J Renew Sustain Energy*. 2013;5:023107. doi:10.1063/1.4794962
133. Yadav V, Kumar Y, Agrawal H, Yadav A. Thermal performance evaluation of solar cooker with latent and sensible heat storage unit for evening cooking. *Aust J Mech Eng*. 2017;15:93-102. doi:10.1080/14484846.2015.1093260
134. Bhave AG, Thakare KA. Development of a solar thermal storage cum cooking device using salt hydrate. *Sol Energy*. 2018;171:784-789. doi:10.1016/j.solener.2018.07.018
135. Mawire A, Lentswe K, Owusu P, et al. Performance comparison of two solar cooking storage pots combined with wonderbag slow cookers for off-sunshine cooking. *Sol Energy*. 2020;208:1166-1180. doi:10.1016/j.solener.2020.08.053
136. Hussein HMS, El-Ghetany HH, Nada SA. Experimental investigation of novel indirect solar cooker with indoor PCM thermal storage and cooking unit. *Energy Conver Manag*. 2008;49:2237-2246. doi:10.1016/j.enconman.2008.01.026
137. Sharma SD, Iwata T, Kitano H, Sagara K. Thermal performance of a solar cooker based on an evacuated tube solar collector with a PCM storage unit. *Sol Energy*. 2005;78:416-426. doi:10.1016/j.solener.2004.08.001
138. Merlin K, Soto J, Delaunay D, Traonvouez L. Industrial waste heat recovery using an enhanced conductivity latent heat thermal energy storage. *Appl Energy*. 2016;183:491-503. doi:10.1016/j.apenergy.2016.09.007
139. Kaizawa A, Kamano H, Kawai A, et al. Thermal and flow behaviors in heat transportation container using phase change material. *Energy Conver Manag*. 2008;49:698-706. doi:10.1016/j.enconman.2007.07.022
140. Nomura T, Okinaka N, Akiyama T. Waste heat transportation system, using phase change material (PCM) from steelworks to chemical plant. *Resour Conserv Recycl*. 2010;54:1000-1006. doi:10.1016/j.resconrec.2010.02.007
141. Koide H, Kurniawan A, Takahashi T, et al. Performance analysis of packed bed latent heat storage system for high-temperature thermal energy storage using pellets composed of micro-encapsulated phase change material. *Energy*. 2022;238:121746. doi:10.1016/j.energy.2021.121746
142. Nardin G, Meneghetti A, Dal Magro F, Benedetti N. PCM-based energy recovery from electric arc furnaces. *Appl Energy*. 2014;136:947-955. doi:10.1016/j.apenergy.2014.07.052
143. Dal Magro F, Jimenez-Arreola M, Romagnoli A. Improving energy recovery efficiency by retrofitting a PCM-based technology to an ORC system operating under thermal power fluctuations. *Appl Energy*. 2017;208:972-985. doi:10.1016/j.apenergy.2017.09.054

How to cite this article: Sinaga R, Darkwa J, Omer SA, Worall M. The microencapsulation, thermal enhancement, and applications of medium and high-melting temperature phase change materials: A review. *Int J Energy Res*. 2022;1-42. doi:10.1002/er.7860